MCDONNELL DOUGLAS TECHNICAL SERVICES CO.
HOUSTON ASTRONAUTICS DIVISION

SPACE SHUTTLE ENGINEERING AND OPERATIONS SUPPORT

WORKING PAPER NO. 1.4-7-229

PRIMARY REACTION CONTROL SYSTEM/REMOTE MANIPULATOR SYSTEM INTERACTION WITH LOADED ARM

MISSION PLANNING, MISSION ANALYSIS, AND SOFTWARE FORMULATION

---

23 May 1978

This Working Paper is Submitted to NASA Under Task Order No. D0937, Task Assignment, Contract NAS 9-15550.

PREPARED BY: E. C. Taylor
E. C. Taylor
488-5660, Ext. 257

PREPARED BY: J. D. Davis
J. D. Davis
488-5660, Ext. 257

APPROVED BY: R. T. Theobald
R. T. Theobald
PDRS Analyses
Task Manager
488-5660, Ext. 257

APPROVED BY: T. H. Wenglinski
T. H. Wenglinski
Powered Flight,
Separation and Consumables
Technical Manager
488-5660, Ext. 228

LIST OF FIGURES

FIGURE	TITLE	PAGE
1	Orbiter Body Coordinate System	4
2	RMS Coordinate Systems	6
3	RCS Thruster Locations and Plume Directions	12
4	Thrust Profiles from PRCS Minimum Impulse Firing	13
5	Payload Relative Positions For Step Input Analysis	15
6	Acceleration Histories For Step Input Analysis	18
7	Load History For Positive Roll Maneuver (P.L. in "YORB" Config.)	21
8	Load History For Positive Pitch Maneuver (P.L. in "YORB" Config.)	22
9	Load History For Roll and Positive Yaw Maneuver (P.L. in "YORB" Config.)	23
10	Load History For Roll and Positive Yaw Manuever (P.L. in "YORB" Config.)	24
11	Payload Relative Positions for Minimum Impulse Analysis	26
12	Analytical Model of Orbiter/RMS/ Payload System	28
13	Moments about Shoulder Yaw Joint due to Single Minimum Impulse Firing	31
14	Moments about Shoulder Pitch Joint due to Single Minimum Impulse Firing	32
15	Moments about Elbow Pitch Joint due to Single Minimum Impulse Firing	33
16	Moments about Wrist Pitch Joint due to Single Minimum Impulse Firing	34

FIGURE	TITLE	PAGE
17	Moments about Wrist Yaw Joint due to Single Minimum Impulse Firing	35
18	Moments about Tip of End Effector due to Single Minimum Impulse Firing	36
19	End Effector Response to Pulse Train Input - All Pulses in Positive Direction ($T_o = T_k$)	38
20	End Effector Response to Pulse Train Input - Alternate Pulses ($T_o = T_k$)	39
21	End Effector Response to Pulse Train Input - Alternate Pulses ($T_o = 2\ T_k$)	40
22	End Effector Response to Pulse Train Input - Alternate Pulses ($T_o = 3\ T_k$)	41
23	End Effector Response to Pulse Train input - Alternate Pulses ($T_o = 4\ T_k$)	42
24	Wrist Yaw Joint Drive Axis Loads due to Pulse Inputs about Orbiter y Axis.	43
25	Elbow Pitch Joint Cross Axis Loads due to Pulse Inputs about Orbiter y Axis.	44
26	Shoulder Yaw Joint Cross Axis Loads due to Pulse Inputs about Orbiter y Axis.	45

LIST OF TABLES

TABLE	TITLE	PAGE
1	SPAR Operational Loads	7-8
2	Orbiter Characteristics for PRCS Rotational Maneuvers	11
3	Orbiter Mass Properties	17
4	Payload Mass Properties	17
5	RMS Configuration	17
6	Comparative Data from SPAR and PDRSS Step Input Analyses	19
7	Summary of Load Responses to Pulse Train Inputs	46

TABLE OF CONTENTS

	PAGE
LIST OF FIGURES	ii
LIST OF TABLES	iv
1.0 Summary	1
2.0 Introduction	3
3.0 System Definition	4
3.1 Coordinate systems	4
3.2 Structural Load Limits	5
3.3 PRCS Minimum Impulse	9
4.0 Analysis and Results	14
4.1 Step Input Analysis	14
4.1.1 Assumptions and Constraints	14
4.1.2 Results	16
4.2 Minimum Impulse Analysis	25
4.2.1 Assumptions and Constraints	25
4.2.2 Analytical Approach	25
4.2.3 Results	29
5.0 Conclusions and Recommendations	47
6.0 References	48

1.0 Summary

This working paper documents a study of the interaction between the orbiter primary reaction control system (PRCS) and the remote manipulator system (RMS) with a loaded arm. This analysis was performed with the Payload Deployment and Retrieval Systems Simulation (PDRSS) program with the passive arm bending option. The passive-arm model simulates the arm as massless elastic links with locked joints.

The goals of the study were (1) to provide additional validation of the PDRSS program and (2) to provide analysis data to aid in determining if the PRCS jets can be fired with a loaded arm. The major parameters of concern were the arm joint loads. SPAR operational loads are provided for comparison purposes.

The study was divided into two parts. The first part was the evaluation of the response of the arm to step inputs (i.e. constant jet torques) about each of the orbiter body axes. The joint torques quickly exceeded the SPAR maximum operational loads. For the case with constant torques applied about the orbiter roll axis, the shoulder joint cross-axis reached its maximum operational load in approximately one second. The results from this part of the study were compared with the results of a similar study by SPAR.

The second part of the study was the evaluation of the response of the arm to minimum impulse primary RCS jet firings with both single pulse and pulse train inputs. Single minimum impulses were applied to the orbiter about each of the orbiter body axes and the resulting arm joint torques calculated. The responses to the pitch, roll and yaw maneuvers displayed natural periods of approximately 28, 17, and 14 seconds respectively.

The magnitudes of the loads due to the yaw maneuver were an order of magnitude less than those due to the pitch and roll maneuvers. None of the torques observed exceeded the SPAR mean operational loads.

The results of this study showed that the passive-arm model could be driven unstable with a pulse train of PRCS minimum impulse jet firings. Several different frequencies for pulse train inputs which resulted in divergent arm oscillations were identified and the response of the arm to those inputs was demonstrated. The resulting joint torques were also shown and compared with SPAR mean operational loads. The wrist joint proved to be the most sensitive, reaching its mean operational load after only two pulses had been applied to the orbiter. The results from this part of the study were compared against results predicted by a simplified analytical model.

Section 2 outlines the purpose and goals of the study. Section 3 defines the coordinate systems in which the load data is presented, presents the structural load limits published by SPAR and provides a description of the modeling technique used to simulate the minimum impulse. Section 4 presents the results from the study. Section 5 contains the conclusions and recommendations resulting from the study. Section 6 contains a list of references.

2.0 Introduction

The purpose of this working paper is to present the results of a study of the interaction between the orbiter primary reaction control system (PRCS) and the remote manipulator system (RMS) with a loaded arm. Specifically the study consisted of two parts:

1) Evaluation of the response of the RMS to step inputs (i.e., constant jet torques) about each of the orbiter body axes; and
2) Evaluation of the response of the RMS to minimum impulse jet firings with single pulse and pulse train inputs.

There were two goals for this study. The first was to provide additional validation for the PDRSS model. This was accomplished by comparing the results of part 1 with the results of a similar analysis by SPAR and by comparing the results of part 2 with results predicted by a simplified analytical model. The second goal was to provide analysis data to aid in determining if the PRCS jets can be fired with a loaded arm.

The Payload Deployment and Retreival System Simulation (PDRSS) program (References 1 and 2) with the passive arm bending option was used to perform this analysis. The passive arm model simulates the orbiter and payload as rigid bodies and the RMS arm as massless elastic links with locked joints. A mission situation in which the brakes were on would satisfy the locked joints assumption.

The SVDS milestone 3.11 version of DAPCYC (Reference 3) provided the model of the digital autopilot (DAP) of the onorbit flight control system.

3.0 System Definition

This section defines the coordinate systems in which the load data is presented, presents the load limits published by SPAR and provides a description of the modeling technique used to simulate the minimum impulse.

3.1 Coordinate systems

The load data in this report is presented in several different coordinate systems centered at each of the joints. This section defines the coordinate systems in relation to the orbiter body system shown below in Figure 1.

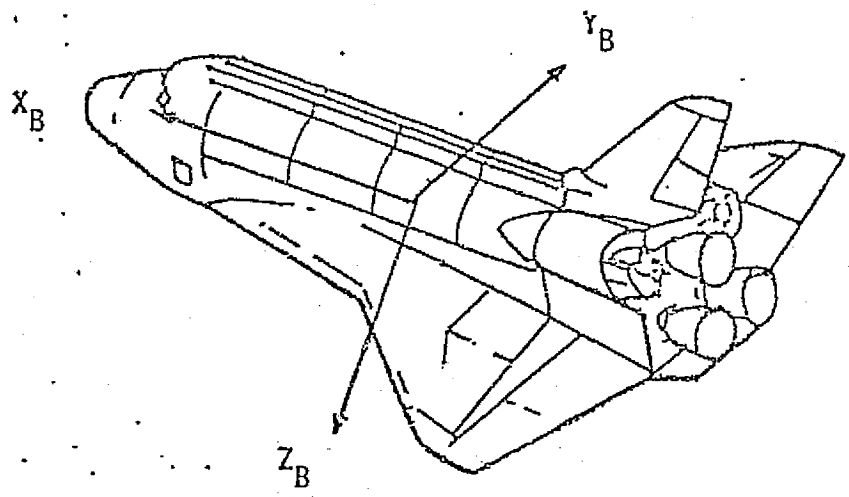

Figure 1: Orbiter Body Coordinate System

The longeron coordinate system (L) is obtained from the orbiter body system by a 180° rotation about the z-axis and a -19.2° rotation about the x axis.

The shoulder yaw coordinate system (SY) is obtained from the longeron system by a rotation of θ_1 degrees about the z-axis where θ_1 is the shoulder yaw angle.

The upper arm coordinate system (UA) is obtained from the shoulder yaw system by a rotation of θ_2 degrees about the y-axis where θ_2 is the shoulder pitch angle.

The lower arm coordinate system (LA) is obtained from the upper arm system by a rotation of θ_3 degrees about the y-axis where θ_3 is the elbow pitch angle.

The wrist coordinate system (WR) is obtained from the lower arm system by a rotation of θ_4 degrees where θ_4 is the wrist pitch angle.

The hand coordinate system (HD) is obtained from the wrist system by a rotation of θ_5 degrees about the z-axis where θ_5 is the wrist yaw angle.

Figure 2 illustrates these coordinate systems with respect to the orbiter body system for the arm configuration used for the minimum impulse analysis

3.2 Structural Load Limits

This section presents the load limits published by SPAR in Reference 7. These loads are provided for comparison purposes. In the following tables, the non-subscripted coordinate systems are SPAR axes. Subscripted axes refer to PDRSS notation as defined in Section 3.1.

Θ_1 = -90.0° = Shoulder Yaw Angle
Θ_2 = 69.0° = Shoulder Pitch Angle
Θ_3 = -19.4° = Elbow Pitch Angle
Θ_4 = 21.1° = Wrist Pitch Angle
Θ_5 = 0.0° = Wrist Yaw Angle

Arm configuration for minimum impulse analysis

B - Orbiter Body Coordinate System
L - Longeron Coordinate System
SY - Shoulder Yaw Coordinate System
UA - Upper Arm Coordinate System
LA - Lower Arm Coordinate System
WR - Wrist Coordinate System
HD - Hand Coordinate System

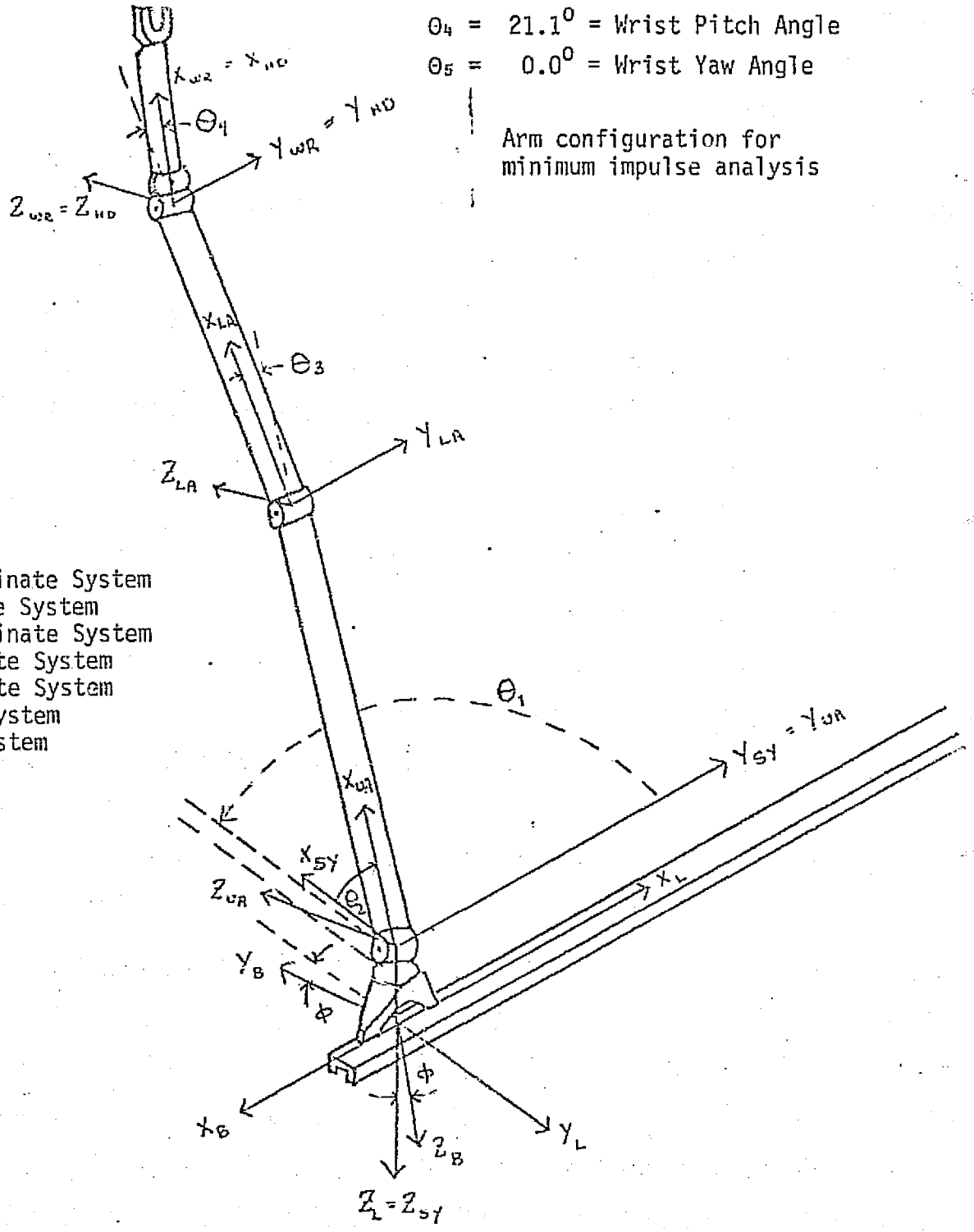

Figure 2: RMS coordinate systems

ORIGINAL PAGE IS OF POOR QUALITY

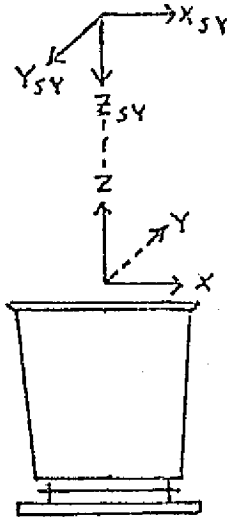

(a) Shoulder Yaw Joint Limit Loads, ft-lbs

Case	Mx	My	Mz*
Mean	1250	1000	1000
Max	1500	1200	1200

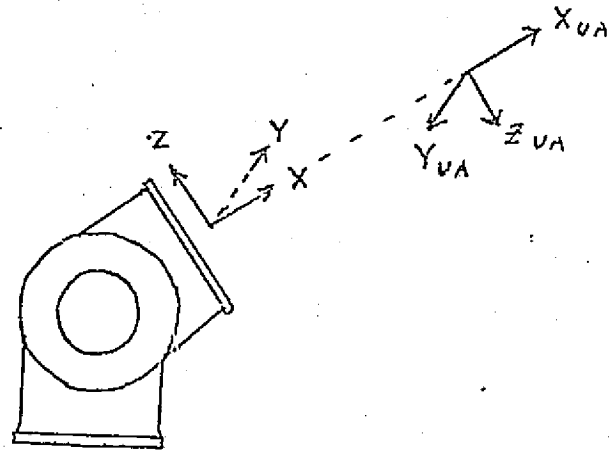

(b) Shoulder Pitch Joint Limit Loads, ft-lbs

Case	Mx	My*	Mz
Mean	1200	1000	1550
Max	1440	1200	1860

* Drive Axis

Table 1: SPAR Operational Loads

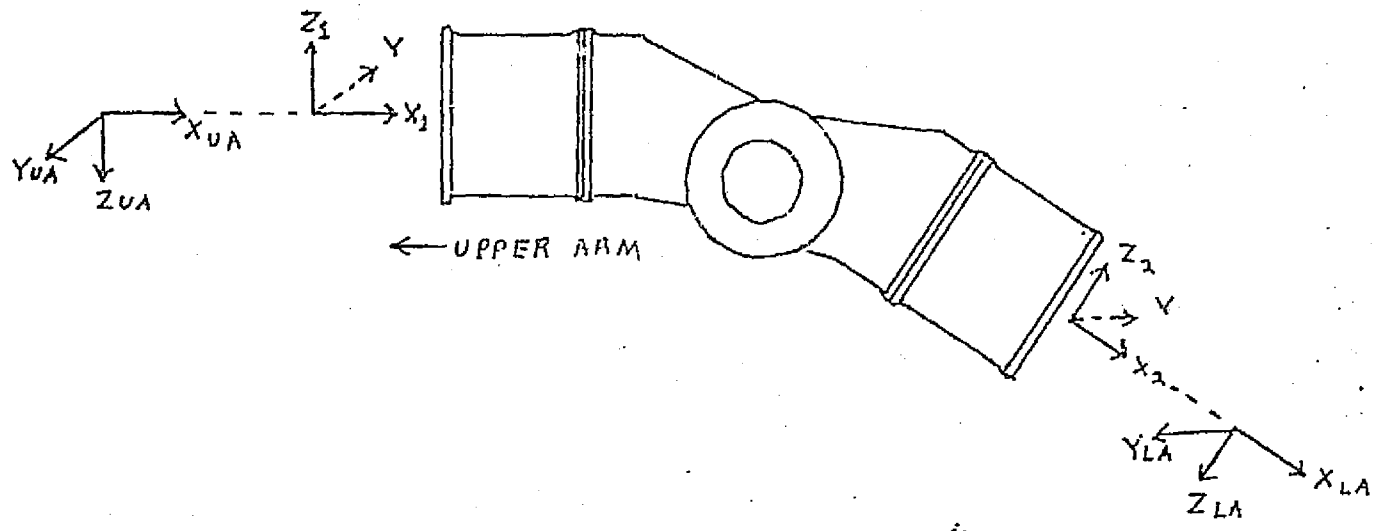

(c) Elbow Joint Limit Loads, ft-lbs

Case	Mx1	Mz1	My*	Mx2	Mz2
Mean	1200	1100	700	300	1350
Max	1440	1320	840	360	1620

(d) Wrist Joint and End Effector Limit Loads, ft-lbs

Case	Mx	My	Mz
Mean	300	300	300
Max	360	360	360

* Drive Axis

Table 1 (cont.): SPAR Operational Loads

3.3 PRCS minimum impulse

This section presents the orbiter characteristics for PRCS rotational maneuvers, describes a minimum impulse PRCS jet firing and describes the technique used to model a minimum impulse with the DAPCYC model (Reference 3).

Table 2 gives the orbiter characteristics for PRCS rotational maneuvers (Reference 4). The positive pitch maneuver uses four jets while the negative maneuver only uses three. This results in a higher orbiter acceleration for a positive pitch maneuver than for a negative one. The positive pitch maneuver was used for the single minimum impulse analysis to allow for the worst case situation.

A minimum impulse jet firing is the result of a single jet-on command from the DAP. The DAP operates at a frequency of 25 hz; therefore, a new command is issued every 40 milliseconds (msec). Figure 4a shows a thrust profile (Reference 5) for a primary RCS thruster for a 40 msec pulse. The rise time for the thrust is 39 msec. It has just reached its steady state value when the jet-off signal is commanded on the next pass through the DAP. The decay time to 10% thrust is another 33 msec.

This profile can be compared with the one output from the DAPCYC model (figure 4b). DAPCYC assumes the thrust magnitude input to the model, normally 100% max thrust, is achieved instantaneously at the jet-on command and the thrust level returns to zero instantaneously at the jet-off command. Using 100% max thrust as the input to the DAPCYC model imparted a higher velocity to the orbiter than those given in Table 2. Therefore an effective thrust level, 71% max thrust, was input to the model. This effective thrust level was found by first integrating the thrust profile in figure 4a to find the total impulse and then dividing the total impulse by one DAP period, 40 msec. The orbiter

velocities achieved using the effective thrust level matched those in Table 2.

TABLE 2: ORBITER CHARACTERISTICS FOR PRCS ROTATIONAL MANEUVERS

Maneuver	Acceleration Levels	Jets*	Orbiter Acceleration at Max Thrust	Orbiter Response Due to Minimum Impulse
+Roll	high	L4D,R4U	1.38 deg/sec^2	3.96 X 10^{-2} deg/sec
-Roll	high	L4U,R4D	-1.38 deg/sec^2	-3.96 X 10^{-2} deg/sec
+Pitch	high	F1D,F2D,L4U,R4U	1.4 deg/sec^2	4.02 X 10^{-2} deg/sec
-Pitch	high	F3U,L4D,R4D	-1.06 deg/sec^2	-3.04 X 10^{-2} deg/sec
+Yaw	high	F1L,R4R	0.777 deg/sec^2	2.23 X 10^{-2} deg/sec
-Yaw	high	F2R,L4L	-0.777 deg/sec^2	-2.23 X 10^{-2} deg/sec

* See Figure 3

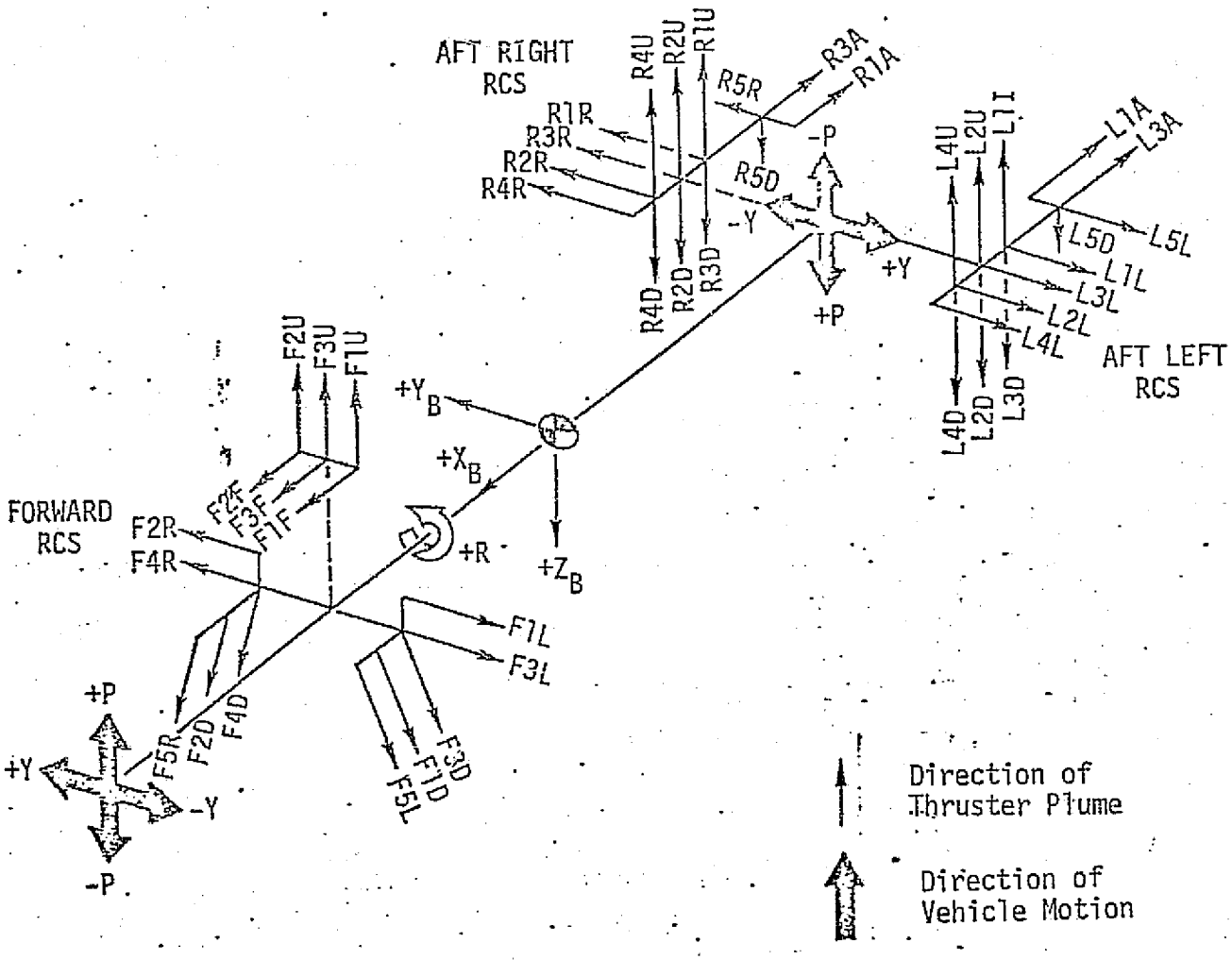

Figure 3: RSC thruster locations and plume directions

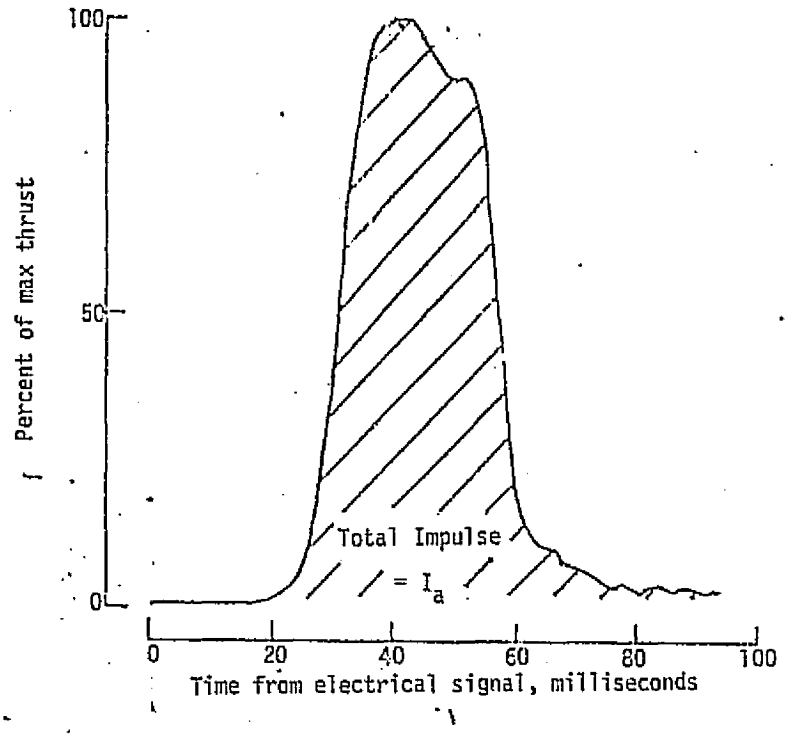

(a) Thrust profile from primary RCS thruster for a 40 msec pulse

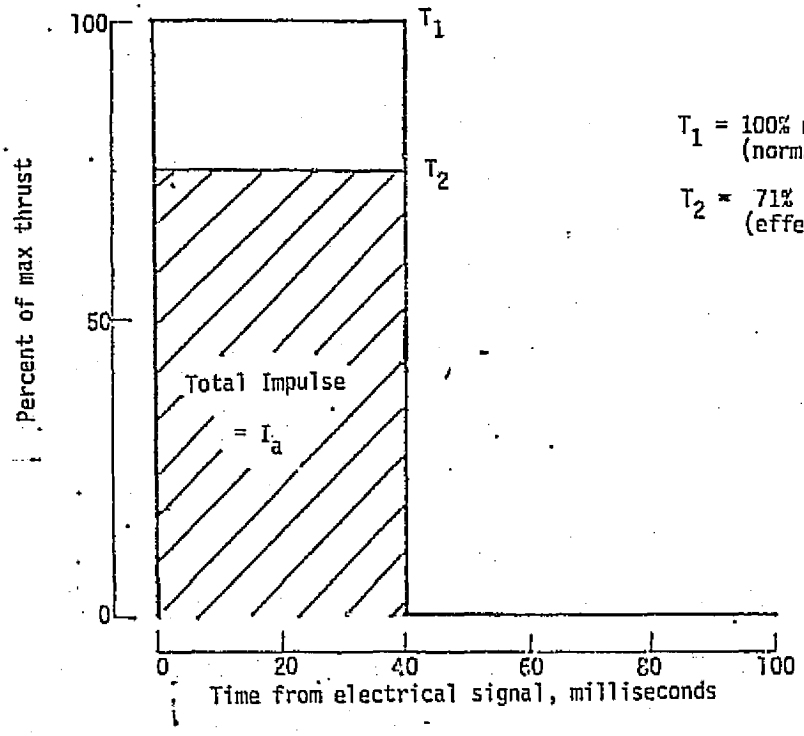

(b) Thrust profile output from DAPCYC model for a 40 msec pulse

Figure 4: Thrust profiles from PRCS minimum impulse firing

4.0 Analysis and Results

This section contains a description of the assumptions and constraints used for this study and also presents the results obtained. Section 4.1 documents the first part of the study, the evaluation of the response of the arm to step inputs. Section 4.2 documents the second part of the study, the evaluation of the response of the arm to minimum impulse jet firings.

4.1 Step input analysis

The purpose or the first part of this study was to evaluate the response of the arm to step inputs. This section presents the results and also contains a comparison between those results and the results obtained in a similar study by SPAR (Reference 8). PDRSS runs made were:

- Positive orbiter pitch with payload in 'XORB' configuration.
- Positive orbiter pitch with payload in 'YORB' configuration.
- Positive orbiter roll with payload in 'XORB' configuration.
- Postive orbiter roll with payload in 'YORB' configuration.
- Positive orbiter yaw with payload in 'XORB' configuration.
- Postive orbiter yaw with payload in 'YORB' configuration.

The 'XORB' and 'YORB' payload configurations are illustrated in Figure 5.

4.1.1 Assumptions and constraints

In order to compare results with SPAR the assumptions and constraints in Reference 8 were duplicated as closely as possible. However, Reference 8 did not specify all of the details of the study. Some unknown details of the SPAR analysis included: constant jet acceleration vs. active DAP

'XORB' Payload Configuration

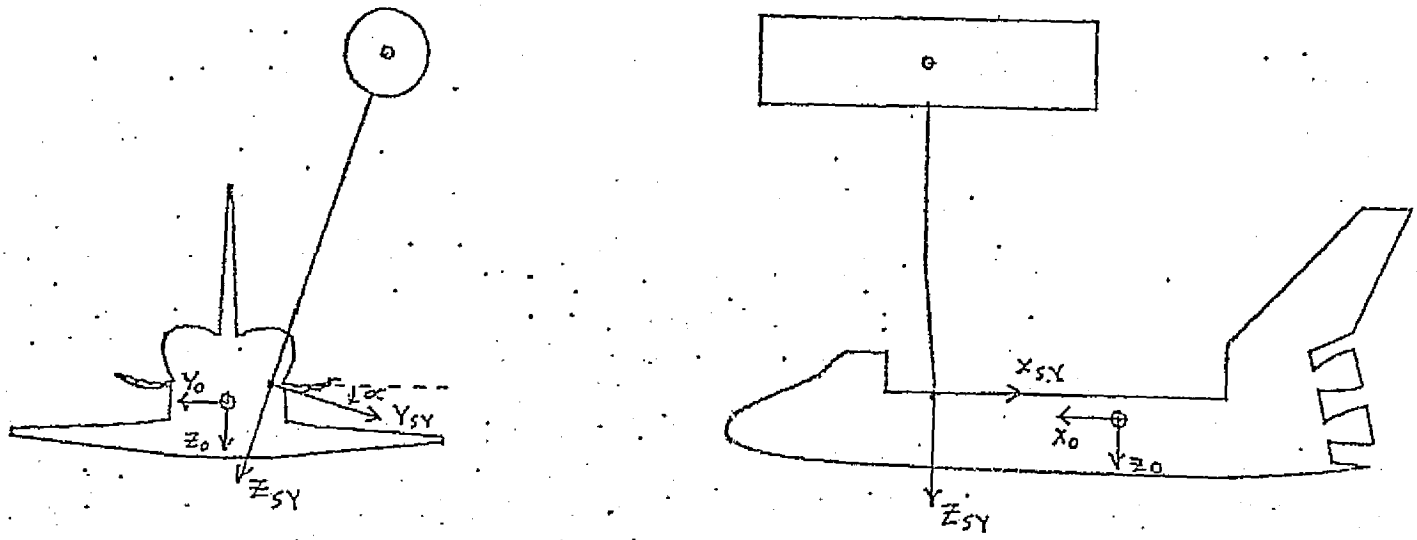

Note: α = ROA = 19.2°

'YORB' Payload Configuration

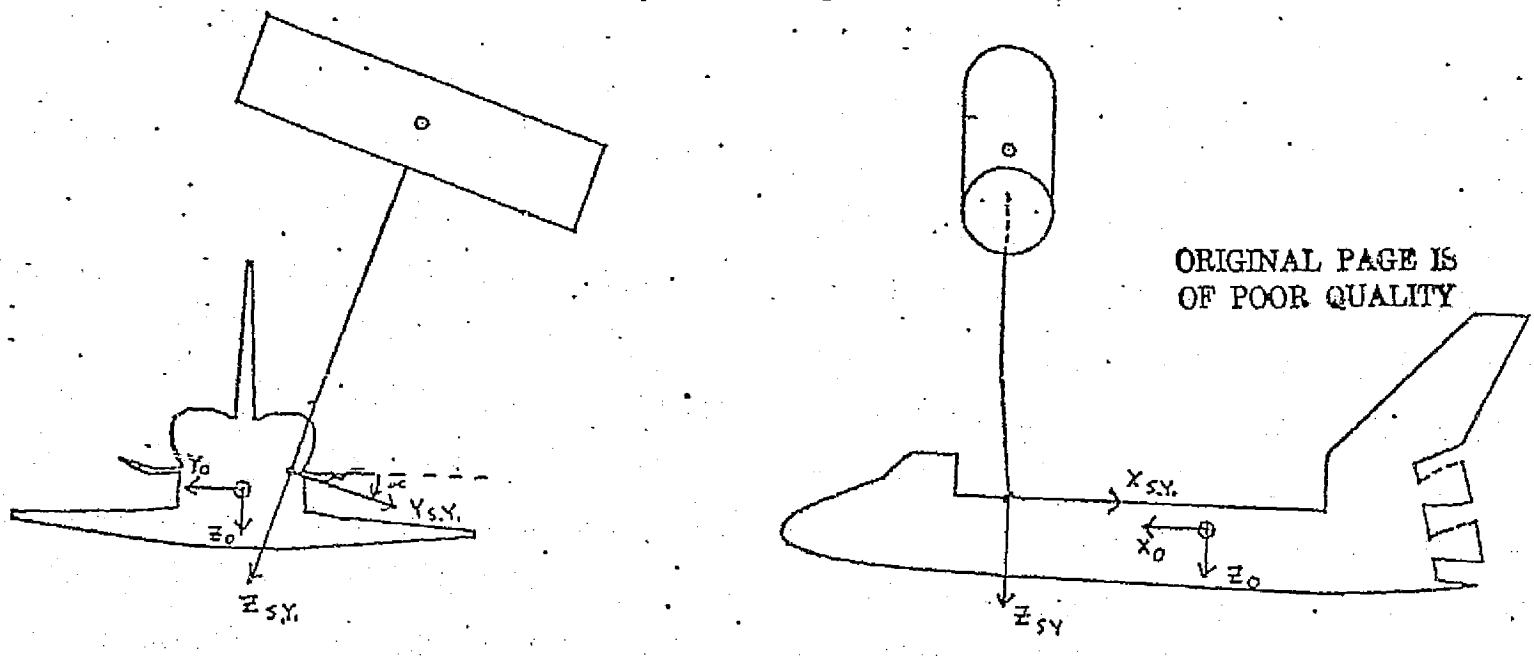

Note : α = ROA = 19.2°

Figure 5: Payload relative positions for step input analysis

(digital autopilot), active joint servo vs. elastic joint model, and payload orientation.

The PRCS jets in the PDRSS program were used to match the "peak" orbiter accelerations listed in Reference 8. The PDRSS runs were made with the DAP on and an elastic joint model. Because of the unknown payload orientation in the SPAR analysis, two payload orientations as shown in Figure 5 were examined. The orbiter and payload mass properties are presented in Table 3 and Table 4, respectively. Table 5 defines the RMS configurations. The RMS configuration used by SPAR is the 'S' configuration. The PDRSS runs used a slightly different arm configuration, as indicated in Table 5, to avoid the singularity associated with 0 degree elbow pitch angle in the PDRSS program.

4.1.2 Results

Figure 6 shows acceleration histories associated with the different maneuvers generated by the PDRSS program. From these acceleration plots one can see that the orbiter rotational acceleration is constantly decreasing due to the flexible arm with payload. The sudden dips in the acceleration curves are due to the DAP jet firings to maintain off-axis attitude hold. For example, a positive roll maneuver requires the DAP to fire jets L4D and L4U (See Figure 3) until the requested roll rate is reached. However, since negative yaw is induced, the positive yaw jets F1L and R4R fire to hold yaw rates and angles within deadbands. These positive yaw jets then induce negative roll which accounts for the sudden decreases in roll acceleration.

Table 6 summarizes the comparisions between the results from this analysis and the results obtained by SPAR.

TABLE 3

ORBITER MASS PROPERTIES

PARAMETER	MAGNITUDE	UNITS
Weight	185,244.	Pounds
I_X	771,000.	Slugs-Ft^2
I_Y	6,013,000.	Slugs-Ft^2
I_Z	6,235,000.	Slugs-Ft^2
I_{XZ}	113,000.	Slugs-Ft^2
I_{XY}	-5000.	Slugs-Ft^2
I_{YZ}	0.0	Slugs-Ft^2
X_{CG}	89.725	Ft
Y_{CG}	0.0	Ft
Z_{CG}	31.175	Ft

TABLE 4

PAYLOAD MASS PROPERTIES

PARAMETER	MAGNITUDE	UNITS
Weight	32,000.	Pounds
Length	60.	Ft
Radius	7.5	Ft
I_{XX}	312,112.	Slugs-Ft^2
I_{YY}	27,973.	Slugs-Ft^2
I_{ZZ}	312,112.	Slugs-Ft^2

TABLE 5

RMS CONFIGURATION

SPAR 'S' Configuration		PDRSS Configuration	
Joint	Angle	Joint	Angle
S.Y.	0	S.Y.	0
S.P.	90o	S.P.	95o
E.P.	0	E.P.	-5o
W.P.	0	W.P.	0
W.Y.	0	W.Y	0
E.E. Roll	0	E.E. Roll	0

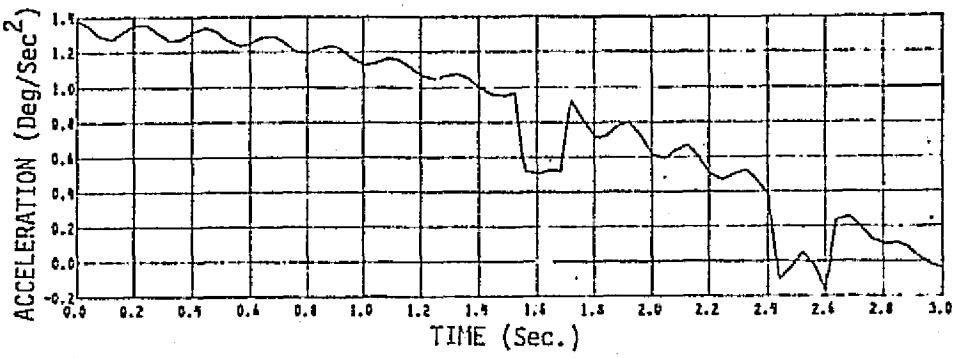

(a.) POSITIVE ROLL MANEUVER: PAYLOAD IN 'YORB' CONFIGURATION

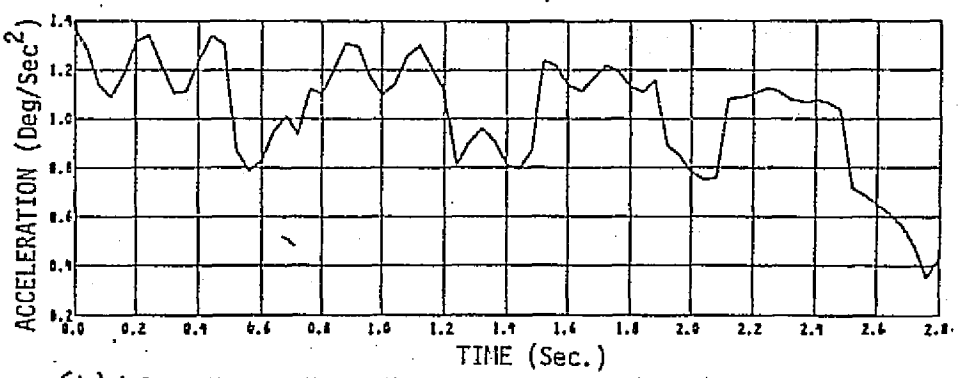

(b.) POSITIVE PITCH MANEUVER: PAYLOAD IN 'XORB' CONFIGURATION

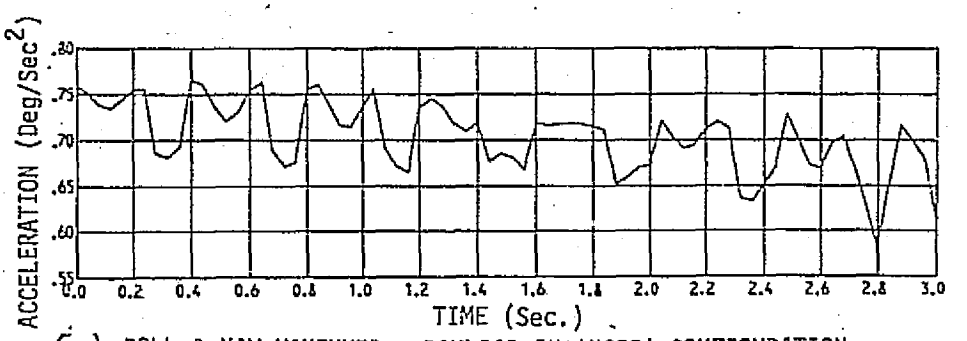

(c.) ROLL & YAW MANEUVER: PAYLOAD IN 'XORB' CONFIGURATION

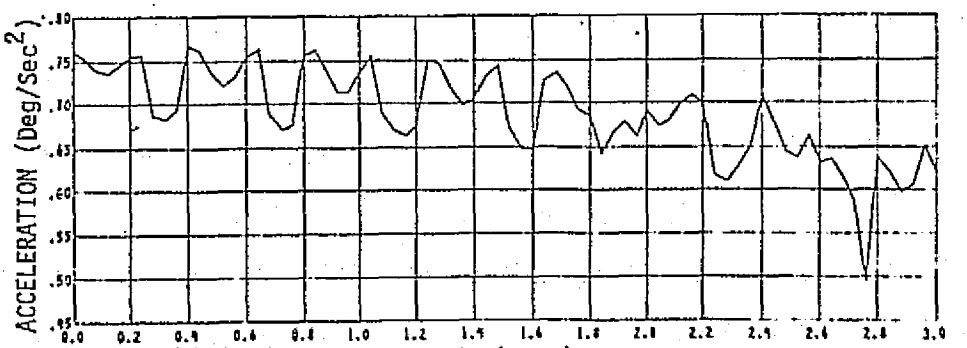

(d.) ROLL & YAW MANEUVER: PAYLOAD IN 'YORB' CONFIGURATION

Figure 6: Acceleration histories for step input analysis

TABLE 6: COMPARATIVE DATA FOR SPAR AND PDRSS INPUT ANALYSIS

SPAR DATA

Maneuver	Acceleration (rad/sec2)	Load $_{TMAX}$ (ft lb)	Orbiter Deflections at TMAX (deg)	TMAX (sec)
Positive Roll	0.024	1500. (M_X)	0.6	1.0
Positive Pitch	0.024	1200. (M_Y)	2.2	1.9
Positive Yaw	0.01356	1200. (M_Y)	1.4	2.05

PDRSS DATA

Maneuver	Payload Position	Initial Acceleration rad/sec2	Load$_{TMAX}$ (ft lb)	Orbiter Deflection at TMAX (deg)	TMAX (sec)
Positive Roll	X ORB	0.024	1500 (M_X)	0.54	0.91
Positive Roll	Y ORB	0.024	1500 (M_X)	0.52	0.89
Positive Pitch	X ORB	0.0238	1200.(M_Y)	0.34	0.75
Positive Pitch	Y ORB	0.0238	1200.(M_Y)	0.35	0.74
Positive Yaw	X ORB	0.0132	1200 (M_Y)	1.03	1.68
Positive Yaw	Y ORB	0.0132	1500 (M_X)	0.91	1.58
Positive Yaw	Y ORB	0.0132	1200 (M_Z)	1.07	1.72

Figures 7-10 present the moment histories for the shoulder yaw joint. The results from the SPAR study are also shown for comparision.

In the positive roll maneuver, the PDRSS runs showed no appreciable difference in the load histories between the 'XORB' and 'YORB' payload configurations. The shoulder yaw joint load history is shown in Figure 7 for the payload in the 'YORB' position. The moment about the x axis in the shoulder yaw joint coordinate system showed the highest moments of the three axes. Initial orbiter acceleration matches that of Reference 8 (0.024 rad/sec^2).

The PDRSS Program was run with a positive pitch maneuver in both 'XORB' and 'YORB' payload configurations with no appreciable difference in the load histories. The load history for the 'XORB' configuration is shown in Figure 8. As expected the moment about the shoulder yaw y axis reached its max design load before the other shoulder moments.

From Reference 8, the roll and yaw maneuver was interpreted as a commanded positive yaw with its associated induced negative roll. For the roll and yaw maneuver with the payload in the 'XORB' configuration the shoulder yaw joint load history is shown in Figure 9. The moment about the shoulder yaw joint y axis reached its max design load before the other shoulder moments. However the PDRSS run reached max torque about the y axis 0.33 seconds before the SPAR run.

For the PDRSS run with the payload in the 'YORB' configuration, the shoulder yaw joint load history is shown in figure 10. However, in this configuration, the moment about y never reaches its max design limit of 1200 ft lb. The moment about x reached its max design limit of 1500 ft lb. first.

Figure 7: Load History For Positive Roll Maneuver - P.L. In 'YORB' Config.

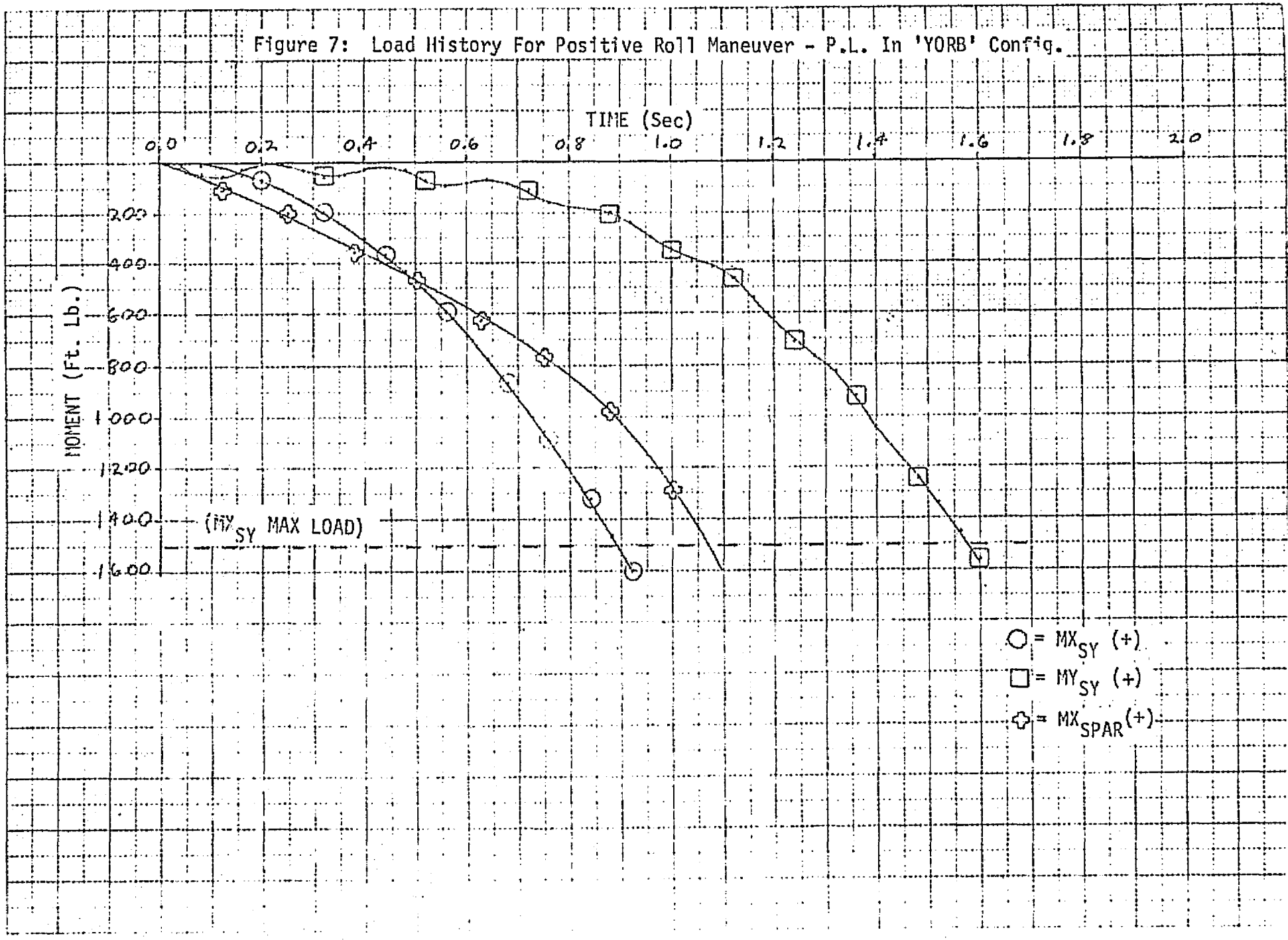

Figure 8: Load History For Positive Pitch Maneuver - P.L. In 'XORB' Config.

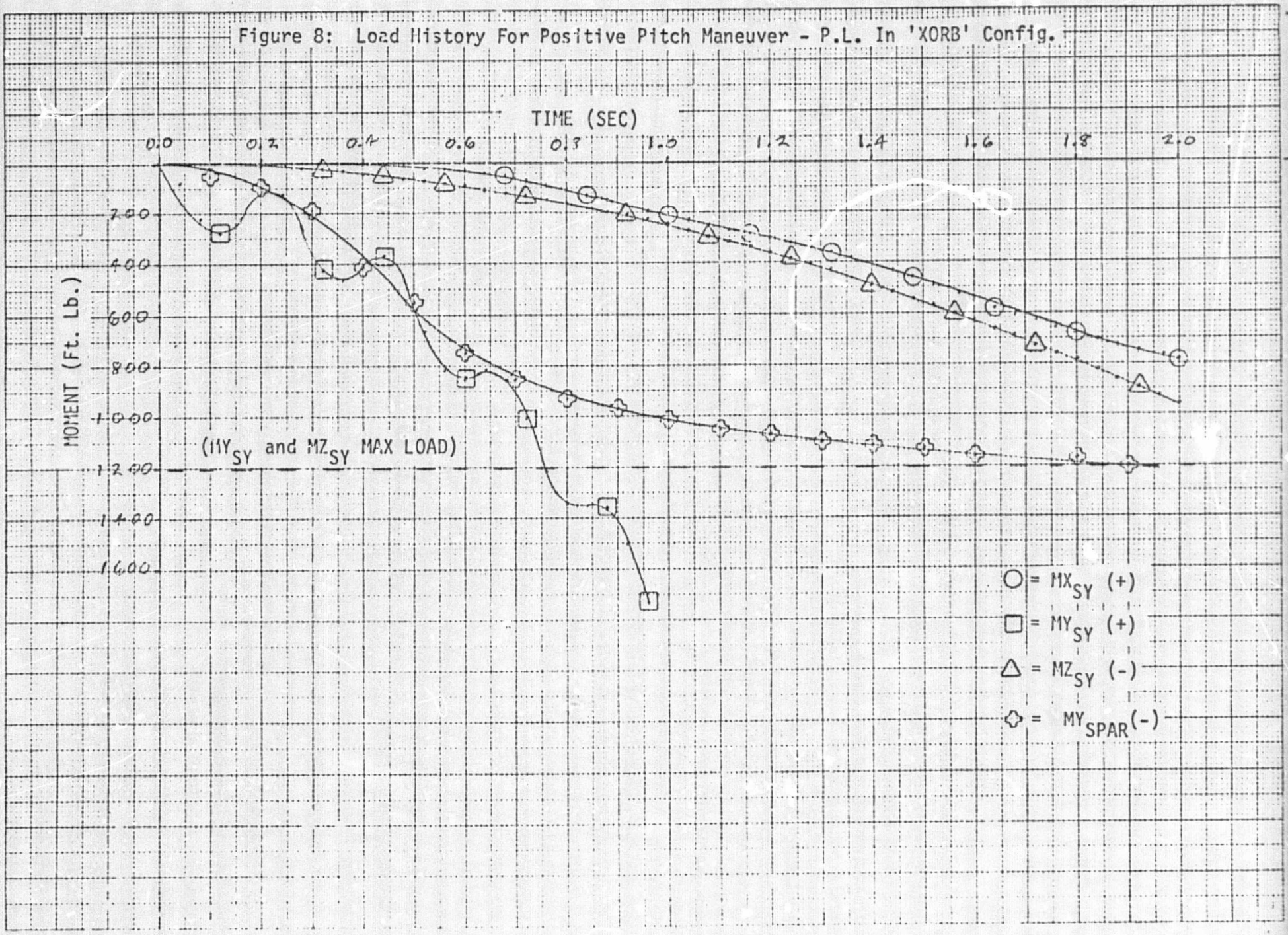

Figure 9: Load History For Roll & Pos. Yaw Maneuver - P.L. In 'XORB' Config.

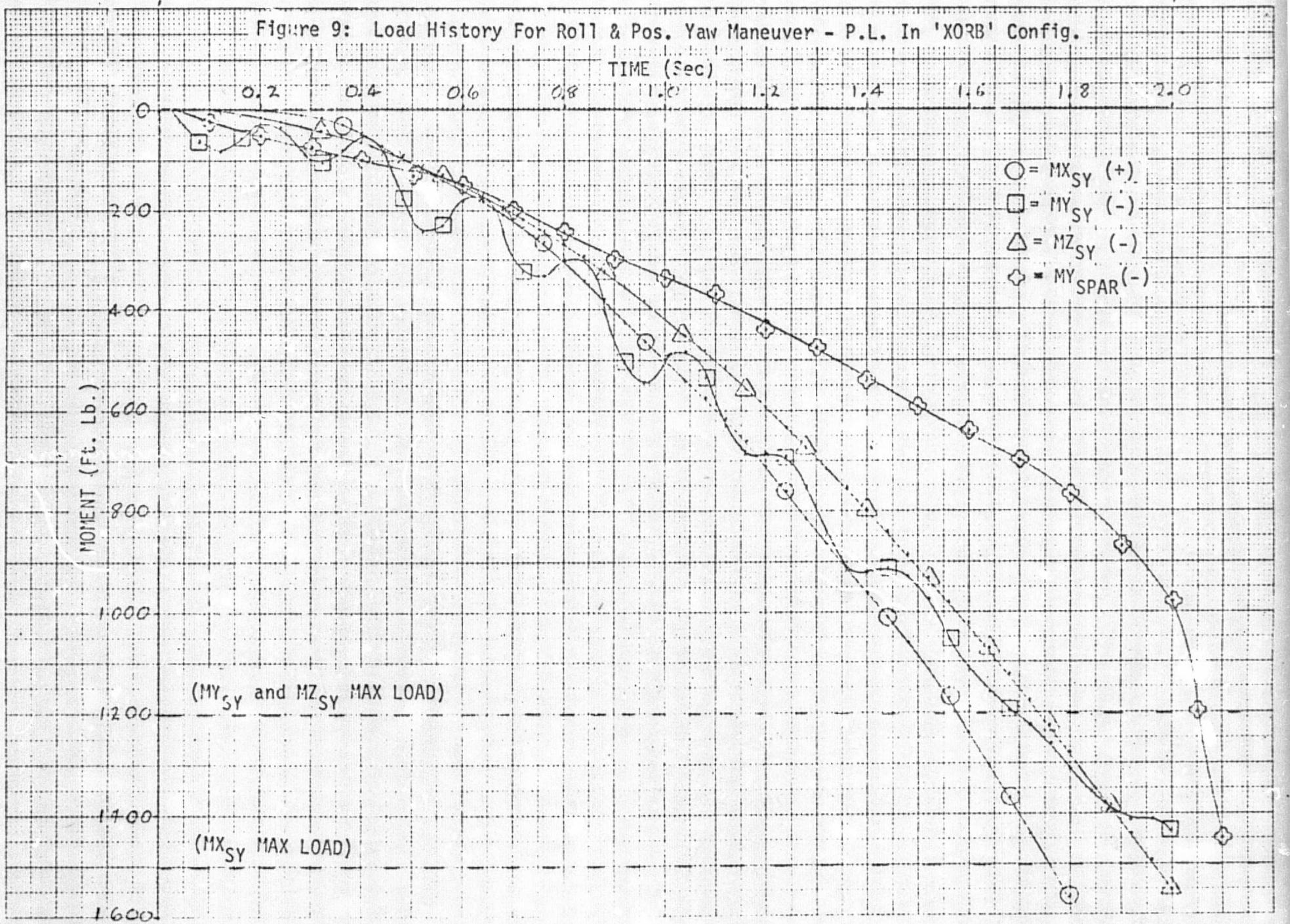

Figure 10: Load History For Roll & Pos. Yaw Maneuver - P.L. In 'YORB' Config.

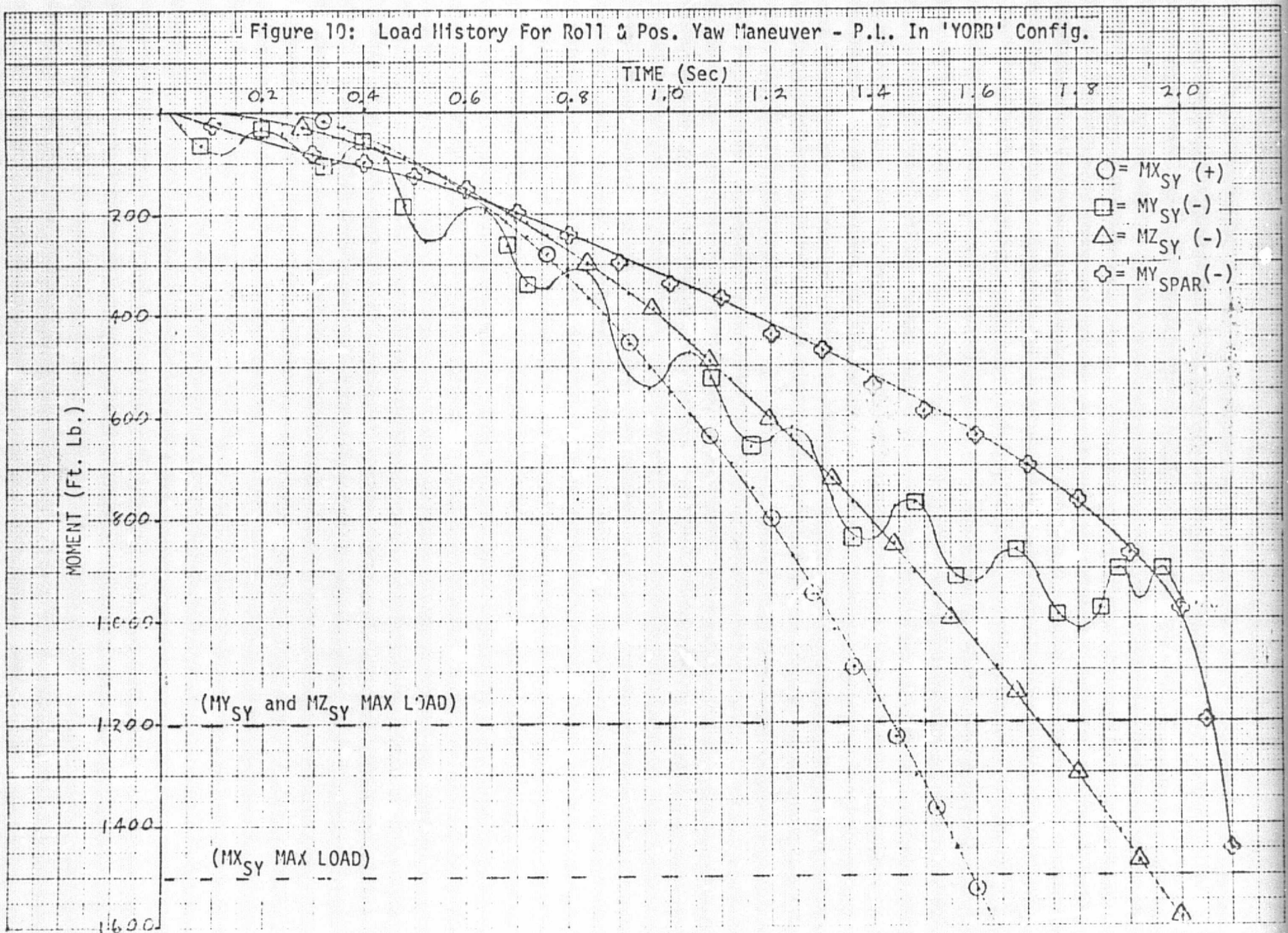

4.2 Minimum impulse analysis

The purpose of the second part of this study was to evaluate the response of the RMS to minimum impulse jet firings. The approach used can be explained in two steps:

1) Input a single minimum impulse about each of the orbiter body axes
   a) Determine the natural frequency of each response
   b) Compare the joint torques with mean operational loads
2) Input pulse trains of different frequencies about the orbiter body pitch axis
   a) Identify frequencies of pulse train inputs which will drive the arm unstable
   b) Compare the joint torques with mean operational loads

4.2.1 Assumptions and constraints

The payload was assumed to be a 32000 lb homogeneous 15' by 60' cylinder. The payload positions relative to the orbiter are shown in figure 11.

The arm angles were initialized as shown in figure 2.

The arm flexibility data was taken from Reference 1.

4.2.2 Analytical approach

An analytical approach was used to predict the response of the arm to pulse trains. The purpose of using a simplified analytical model was twofold. The first was to provide additional validation of the PDRSS program by comparing the results obtained with PDRSS against those predicted by the analytical model. The second was to identify analytically the frequencies of pulse train inputs which will drive the arm unstable.

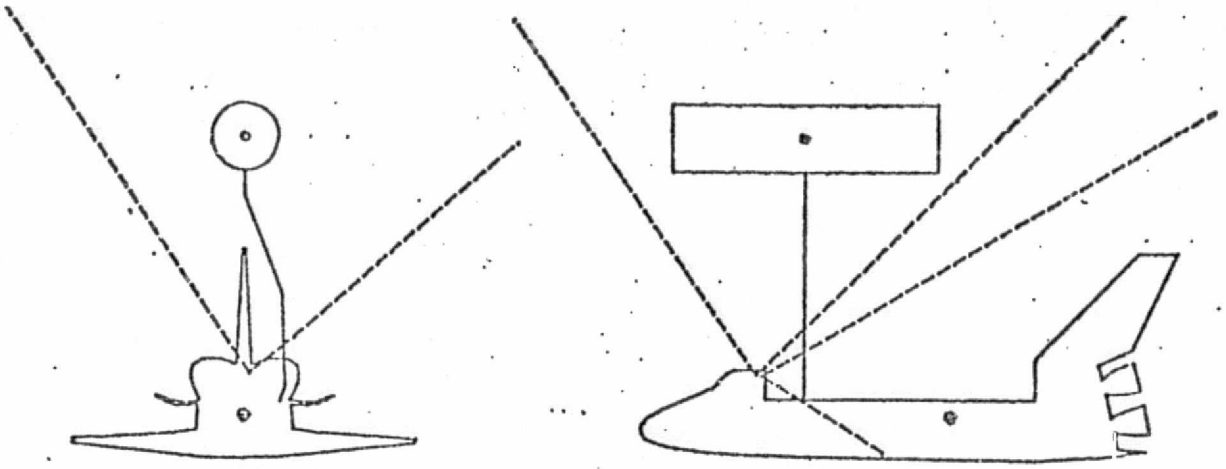

PITCH AND YAW MANEUVERS

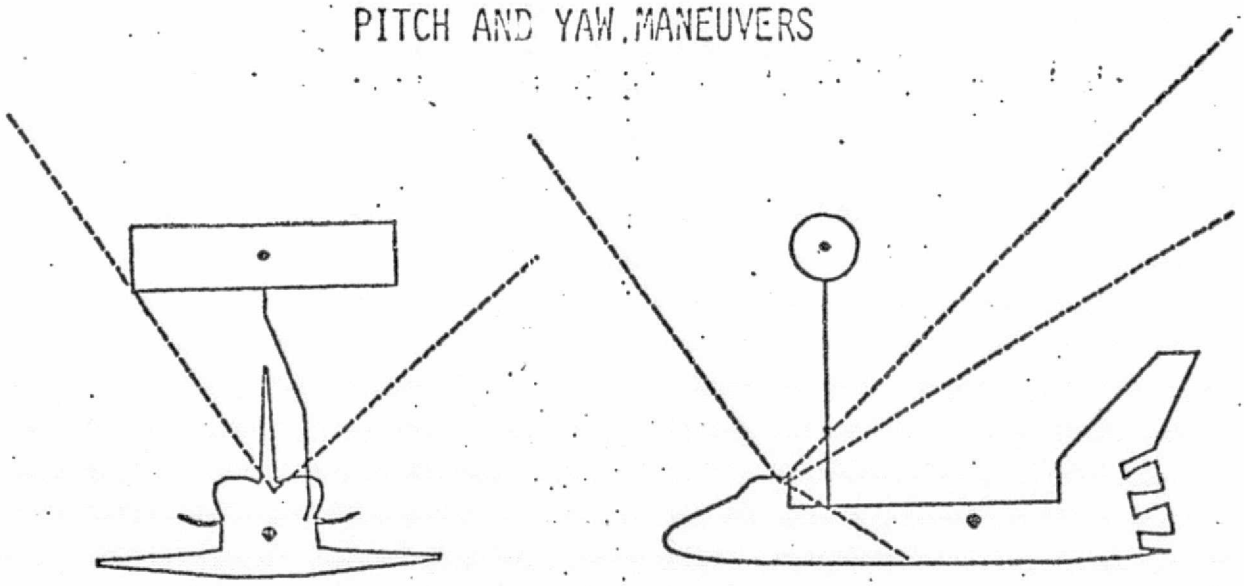

ROLL MANEUVER

Figure 11: Payload relative positions for minimum impulse analysis

The pulse trains (figures 12b and 12c) were input to the simplified analytical model of the orbiter/RMS/payload system developed in Reference 6 and pictured in figure 12a. In this model the orbiter and payload are assumed to be rigid bodies connected by one rigid link with a flexible joint. The link was connected at the CGs of the two bodies. The transfer function of the system is

$$H(S) = \frac{\phi(s)}{X(s)} = \frac{-1}{I_1 \ (s^2 + w_k^2)}$$

where

$$w_k^2 = k\left[\frac{1}{I_1} + \frac{1}{I_2 + m_2 l^2 - \dfrac{m_2^2 l^2}{m_1 + m_2}}\right]$$

Using Fourier analysis techniques the steady state response was computed.

$$\phi(t) = Y_o + \sum_{n=1}^{\infty} 2 \ |Y_n| \cos \ (n w_o t + \angle Y_n)$$

For pulse trains with pulses in the same direction the Fourier coefficients are:

$$Y_o = \frac{-G\ h}{T_o\ I_1\ w_k^2}$$

$$Y_n = \frac{-G\ h\ \mathrm{sinc}(n f_o h)}{T_o\ I_1\ \left[w_k^2 - (2\pi n f_o)^2\right]} \ e^{-j\pi n f_o h} \qquad n = 1,2,3,\ldots$$

$$\text{where } \mathrm{sinc}(x) = \frac{\sin \pi x}{\pi x}$$

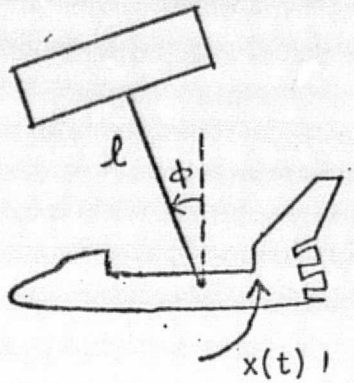

(a) orbiter/RMS/payload system

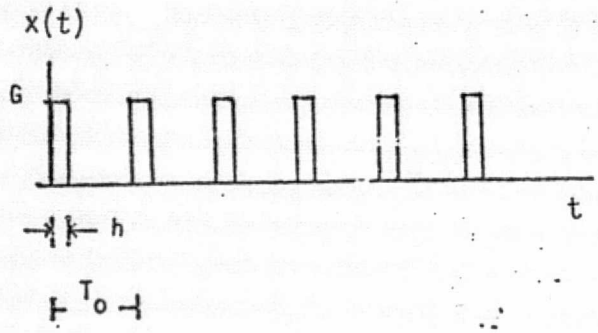

(b) same direction pulse trains

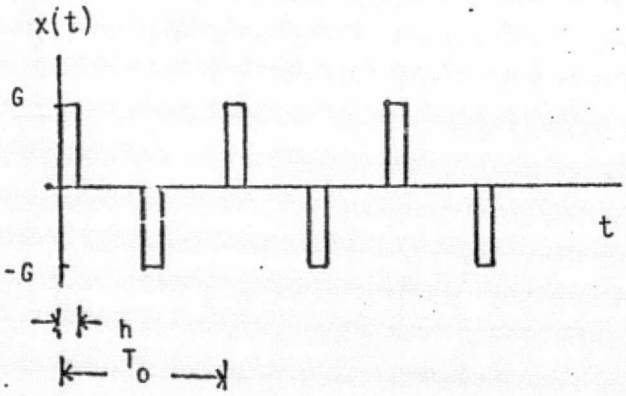

(c) alternate direction pulse trains

m_1 = orbiter mass

$I1$ = orbiter inertia

m_2 = payload mass

$I2$ = payload inertia

k = spring constant

T = joint spring torque = $k\Phi$

w_k = natural frequency of system

T_k = natural period of system

$w_o = 2\pi f_o$ = pulse train frequency

T_o = pulse train period

h = pulse width

G = pulse magnitude

$w_o = 2\pi f_o$ = pulse train frequency

T_o = pulse train period

h = pulse width

G = pulse magnitude

Figure 18: Simplified Analytical Model of Orbiter/RMS/Payload System

The resonant frequencies for same direction pulse trains are those which satisfy the relationship $w_k = nw_o$ or alternately $nT_k = T_o$, $n=1,2,3,...$

For pulse trains with pulses in alternate directions the Fourier coefficients are:

$$Y_o = 0$$

$$Y_n = \frac{-2\ G\ h\ \mathrm{sinc}(nf_o h)}{T_o\ I_1\left[w_k^2 - (2\pi n f_o)^2\right]}\ e^{-j\pi n f_o(h + T_o/2 + \pi/2)} \qquad n=1,3,5,...$$

$$Y_n = 0 \qquad n=2,4,6,...$$

The absense of even harmonics was expected since the alternate pulse trains have halfwave symmetry. The resonant frequencies for alternate pulse trains are those which satisfy the relationship $w_k = nw_o$ or alternately $nT_k = T_o$, $n = 1,3,5...$.

The above analysis shows that for the analytical model same direction pulse trains with periods equal to integer multiples of the system's natural period result in divergent oscillations. Alternate pulse trains with periods equal to odd integer multiples of the system's natural period also result in divergent oscillations. The amplitudes at a given time are twice the amplitudes which result from same direction pulse trains of the same frequency. Alternate pulse trains with periods equal to even integer multiples of the systems natural period do not result in divergent oscillations and have a well-defined steady-state solution.

4.2.3 Results

Figures 13-18 show the torque histories at the arm joints in response to a single minimum impulse. The worst case loads for each maneuver and

for each axis are shown. For example, an impulse about the orbiter pitch axis produces the highest torques at the shoulder yaw joint about the x-axis of the shoulder yaw coordinate system (See figure 2). Also the highest torques about the x-axis of the shoulder yaw system are produced from an impulse about the orbiter pitch axis.

The responses to a single minimum impulse about the orbiter pitch, roll and yaw axes displayed natural periods of approximately 28, 17 and 14 seconds, respectively. The magnitudes of the loads due to an impulse about the orbiter yaw axis were in general an order of magnitude smaller than the loads resulting from the pitch and roll maneuvers. This was expected because the forces exerted by the payload act through a shorter moment arm for the yaw maneuver than for the roll and pitch maneuvers. None of the loads observed exceeded the SPAR mean operational loads.

Pulse trains with periods equal to integer multiples of the system's natural period were applied to the orbiter using the PDRSS program. The resulting end effector responses are shown in figures 19-23. These responses matched the analytical predictions given in Section 4.2.2. Divergent oscillations resulted from same direction pulse trains with $T_o = nT_k$ and alternate direction pulse trains with $T_o = nT_k$, n odd. For alternate direction pulse with $T_o = nT_k$, n even, the oscillations were small and bounded. The ramp present in the response to alternate direction pulse trains was due to the unequal pitch torque magnitudes. (See Section 3.3)

Torque, ft-lbs.
shoulder yaw coordinate system

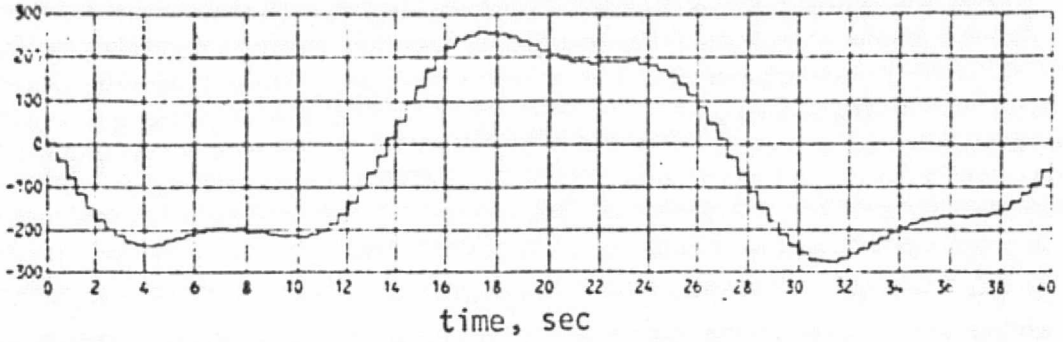

(a) Moment about x due to impulse about orbiter pitch axis

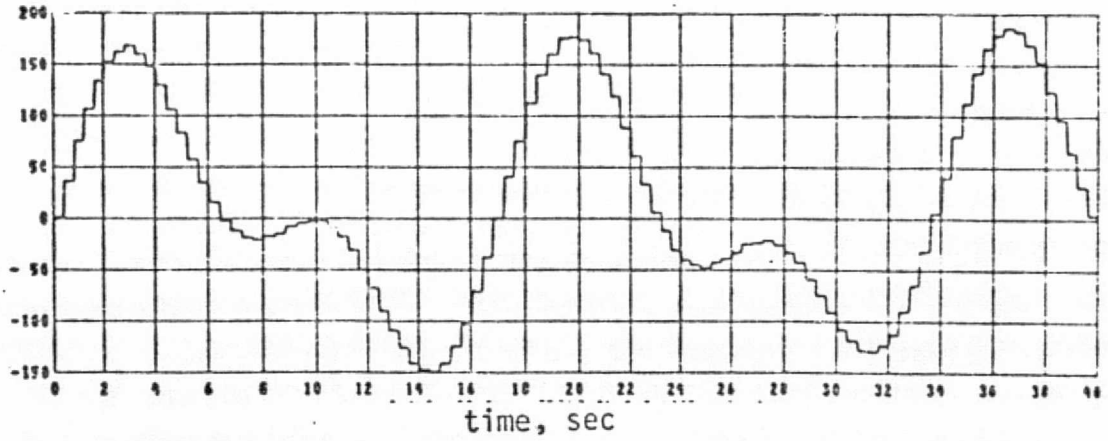

(b) Moment about y due to impulse about orbiter roll axis

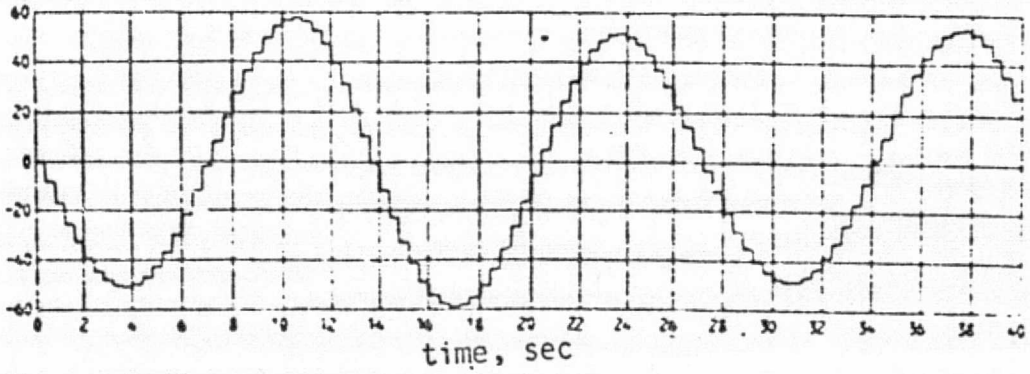

(c) Moment about z due to impulse about orbiter yaw axis

Figure 13: Moments about shoulder yaw joint due to single minimum impulse firing

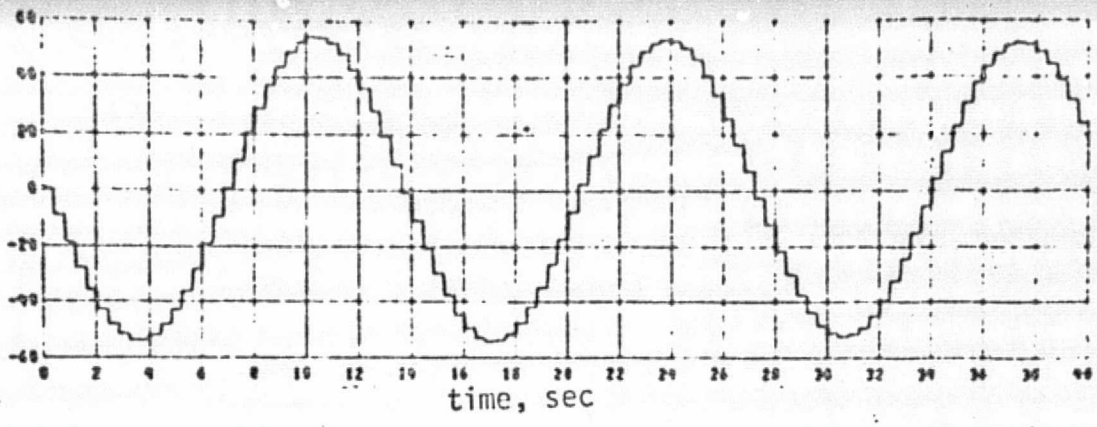

(a) Moment about x due to impulse about orbiter yaw axis

Torque, ft-lbs
upper arm coordinate system

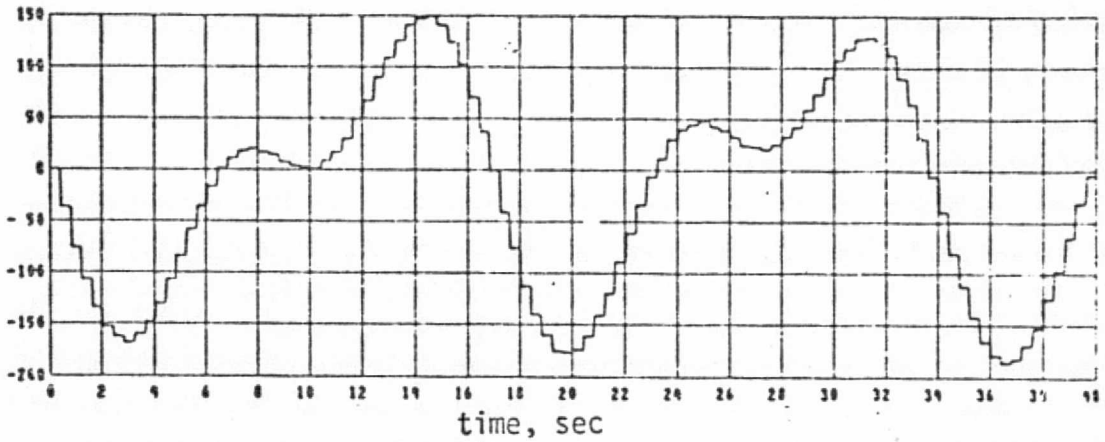

(b) Moment about y due to impulse about orbiter roll axis

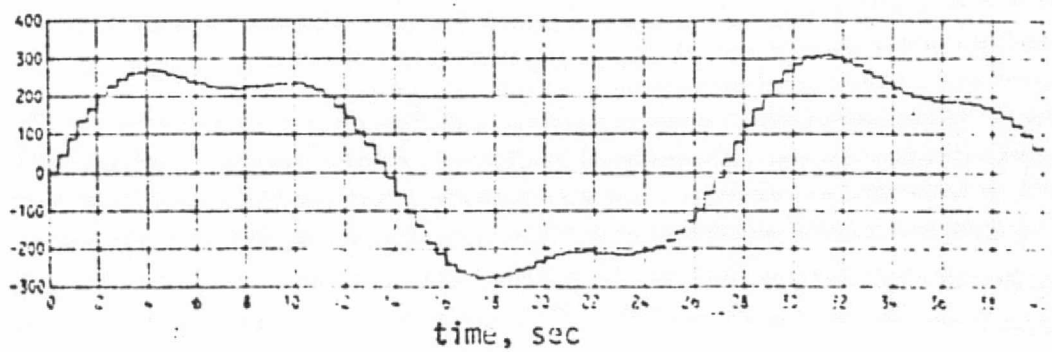

(c) Moment about z due to impulse about orbiter pitch axis

Figure 14: Moments about shoulder pitch joint due to single minimum impulse firing

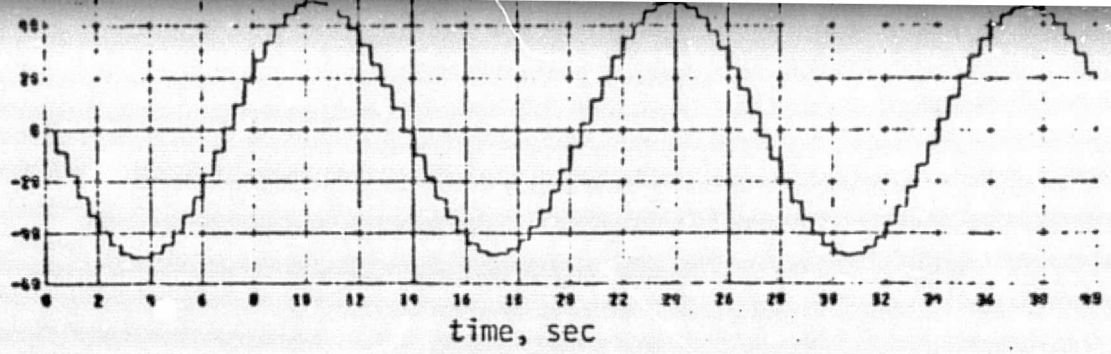

(a) Moment about x due to impulse about orbiter yaw axis

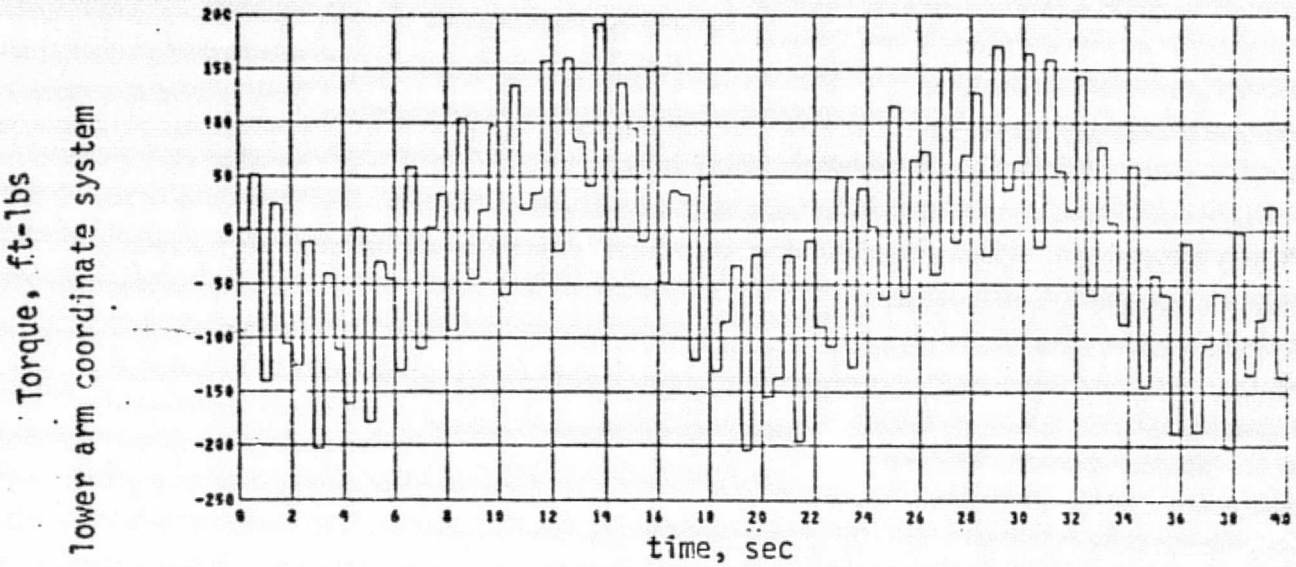

(b) Moment about y due to impulse about orbiter roll axis

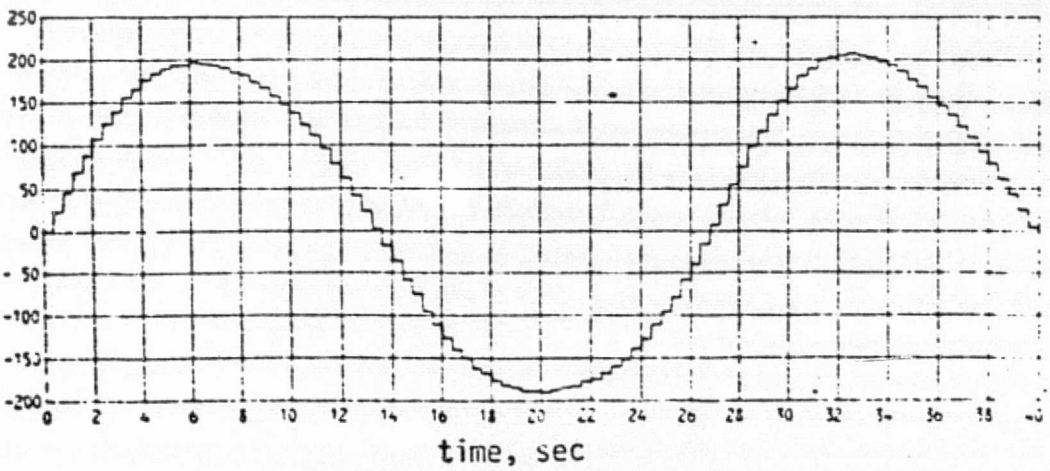

(c) Moment about z due to impulse about orbiter pitch axis

Figure 15: Moments about elbow pitch joint due to single minimum impulse firing

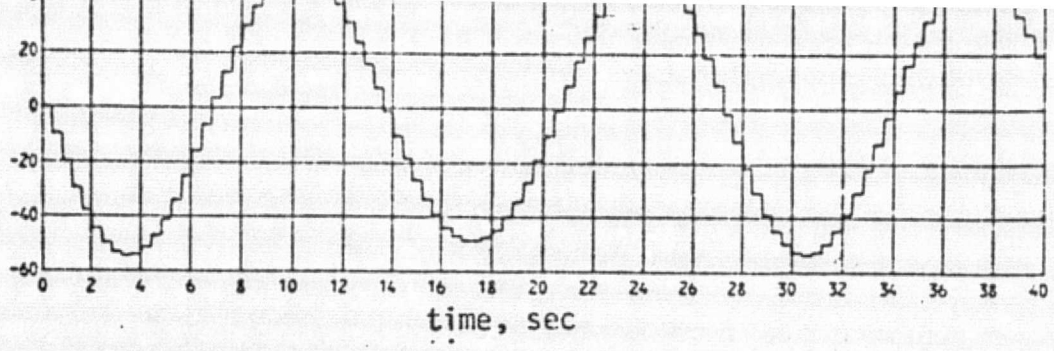

(a) Moment about x due to impulse about orbiter yaw axis

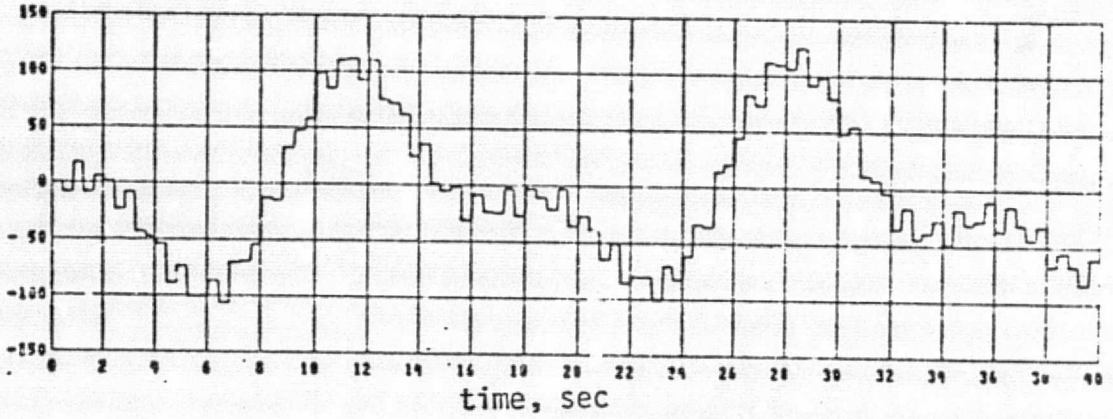

(b) Moment about y due to impulse about orbiter roll axis

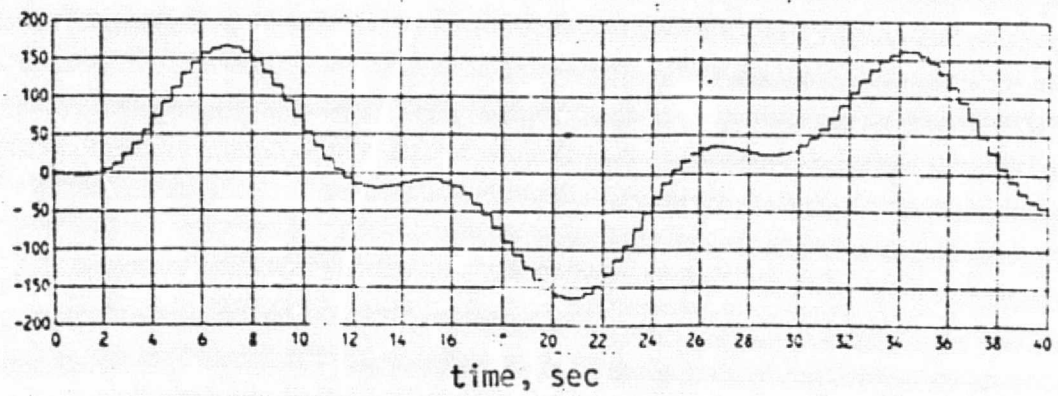

(c) Moment about z due to impulse about orbiter pitch axis

Figure 16: Moments about wrist pitch joint due to single minimum impulse firing

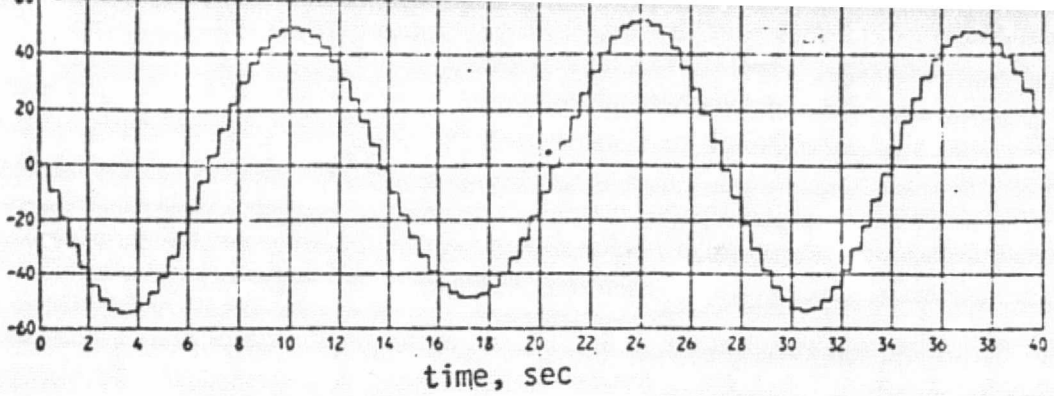

(a) Moment about x due to impulse about orbiter yaw axis

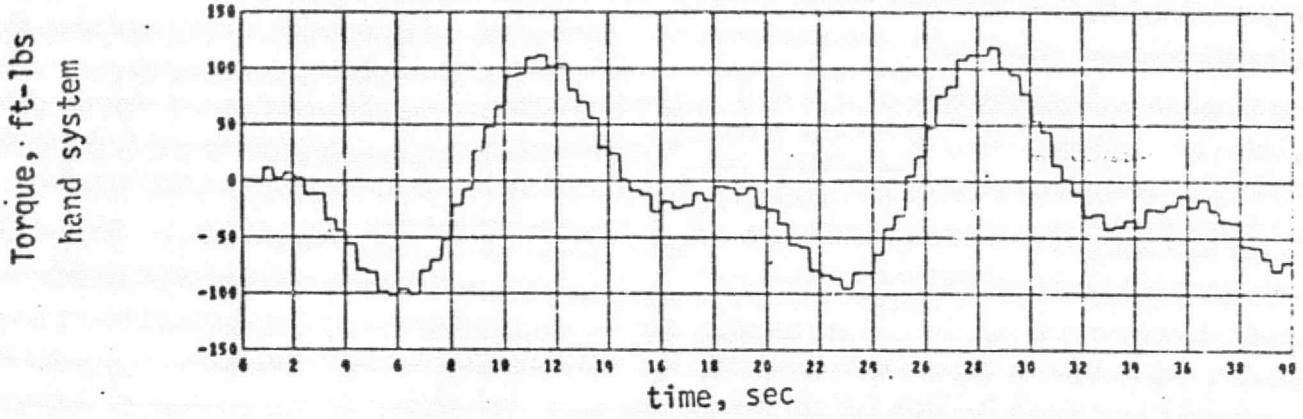

(b) Moment about y due to impulse about orbiter roll axis

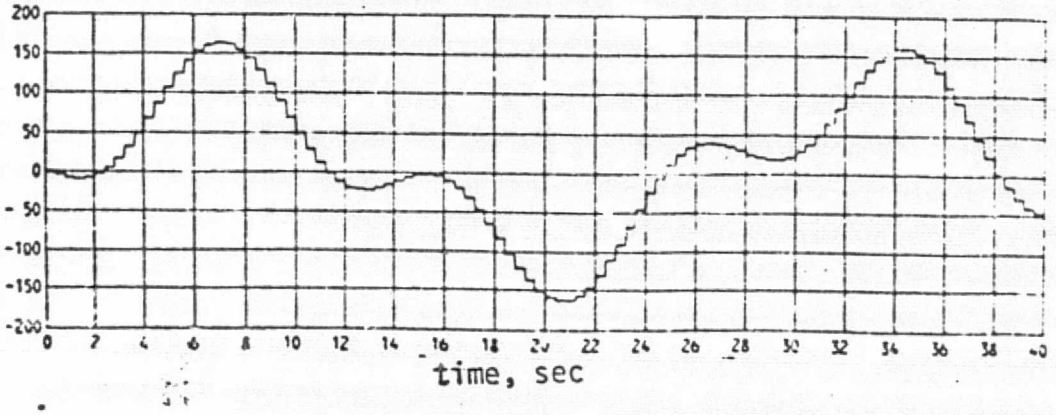

(c) Moment about z due to impulse about orbiter pitch axis

Figure 17: Moments about wrist yaw joint due to single minimum impulse firing

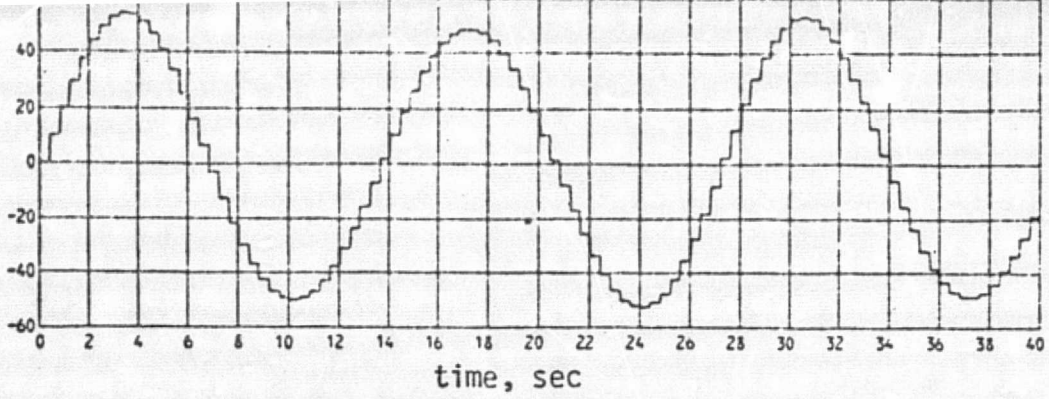

(a) Moment about x due to impulse about orbiter yaw axis

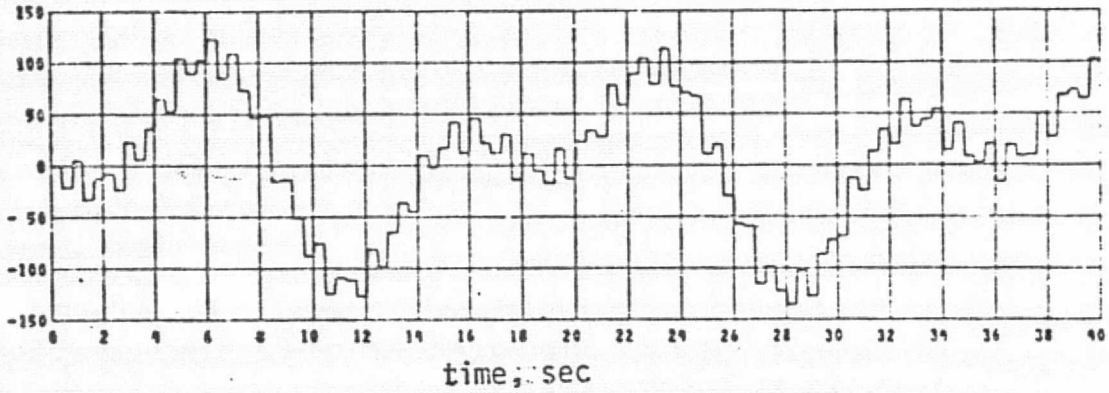

(b) Moment about y due to impulse about orbiter roll axis

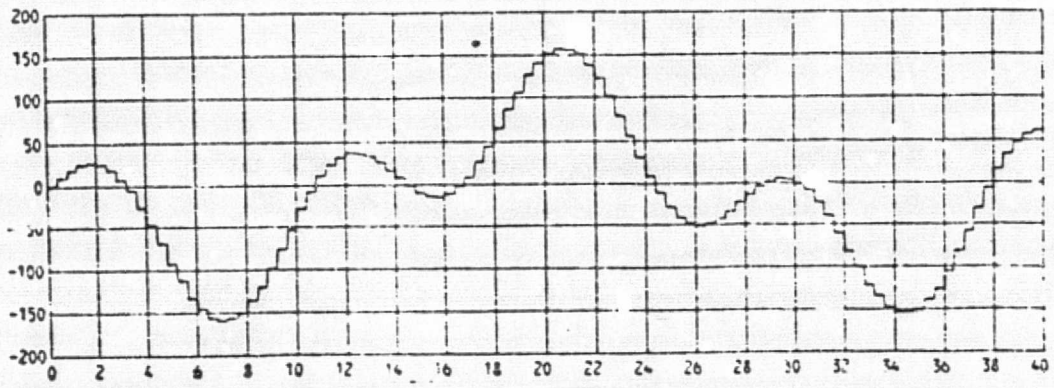

(c) Moment about z due to impulse about orbiter pitch axis

Figure 18: Moments about tip of end effector due to single minimum impulse firing

The results are shown for pitch maneuvers only. Similar results were obtained for pulse trains applied about the orbiter roll axis.

Figures 24-26 show selected joint torque histories for the cases with diverging arm oscillations. The response to a single pulse is also shown for comparison. The tic marks indicate the times at which the pulses were applied. The wrist joint reached its mean operational load after only two pulses had been applied to the orbiter. Table 7 gives a summary for the load histories shown.

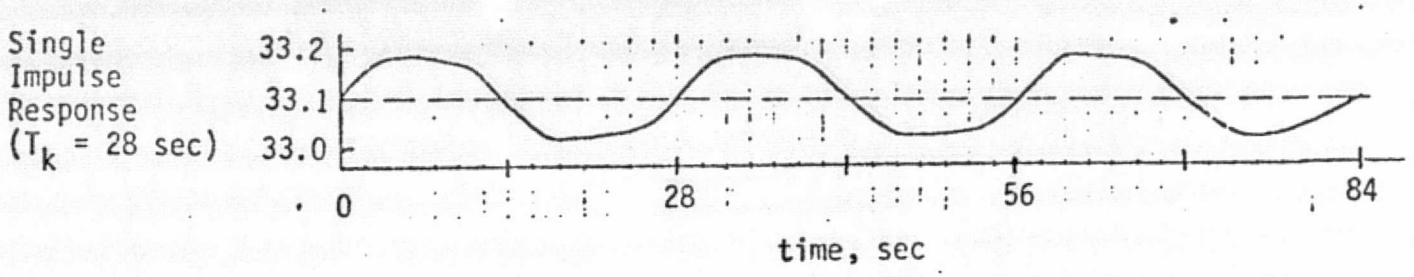

(a) Relative end effector x-position, ft

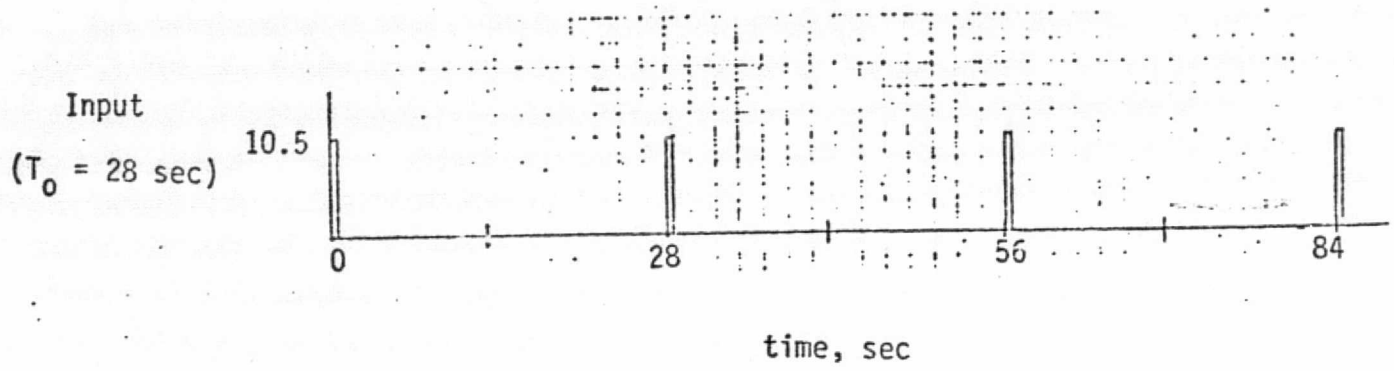

(b) Moment about orbiter y-axis due to PRCS jets, 10^4 ft-lbs

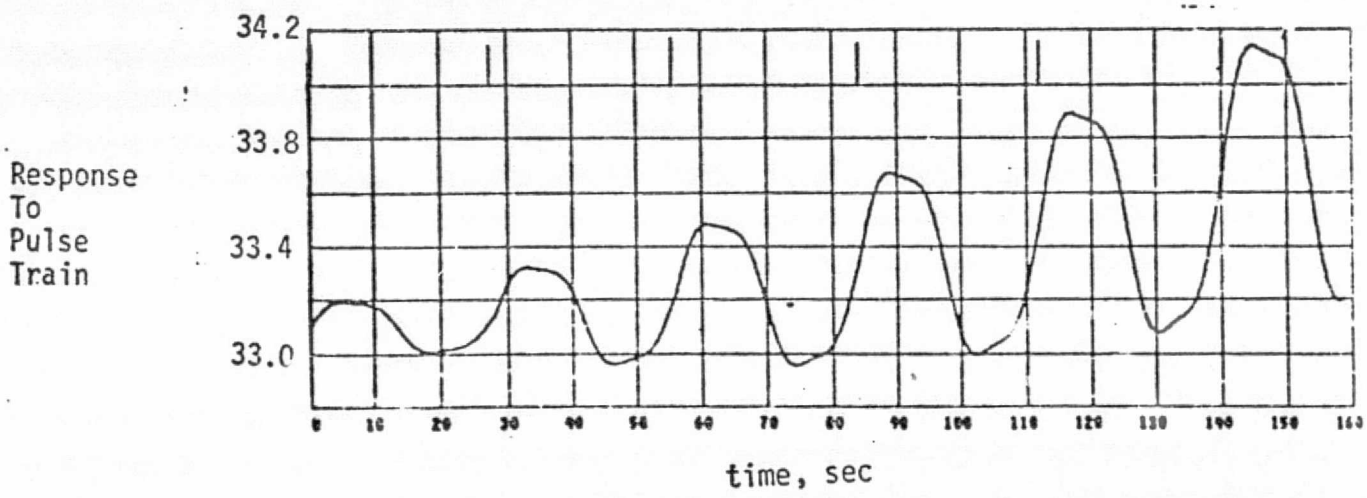

(c) Relative end effector x-position, ft

Figure 19: End effector response to pulse train input
All pulses in positive direction ($T_o = T_k$)

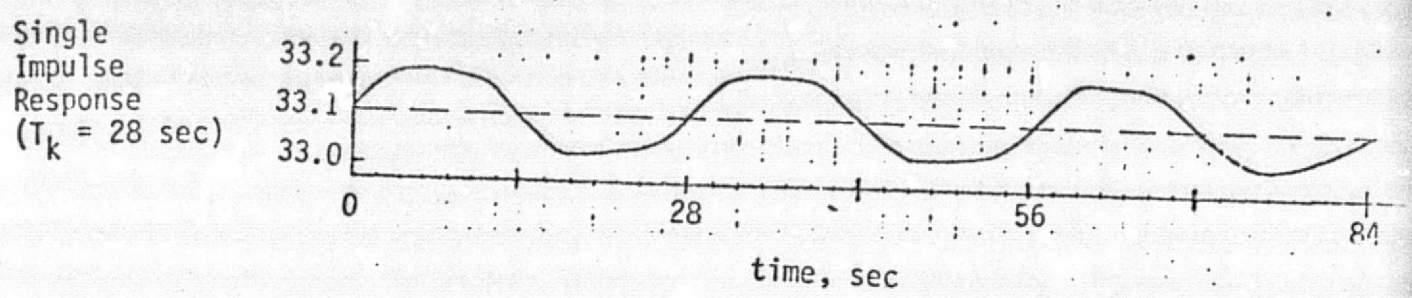

(a) Relative end effector x-position, ft

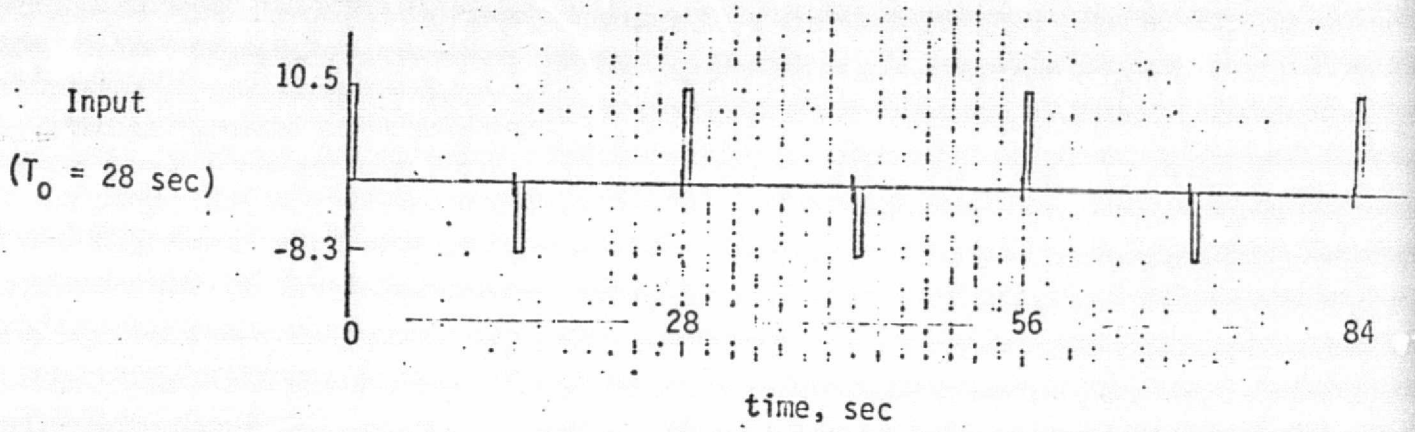

(b) Moment about orbiter y-axis due to PRCS jets, 10^4 ft-lbs

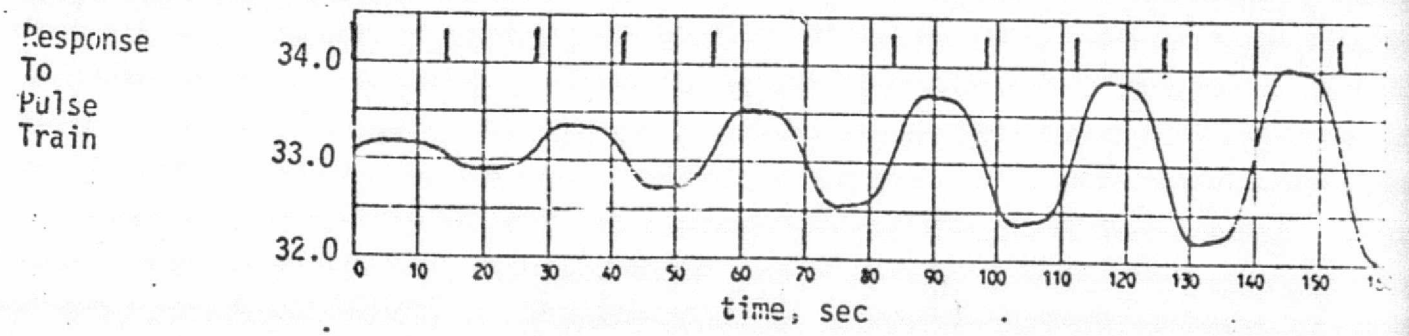

(c) Relative end effector x-position, ft

Figure 20: End effector response to pulse train input
Alternate pulses ($T_o = T_k$)

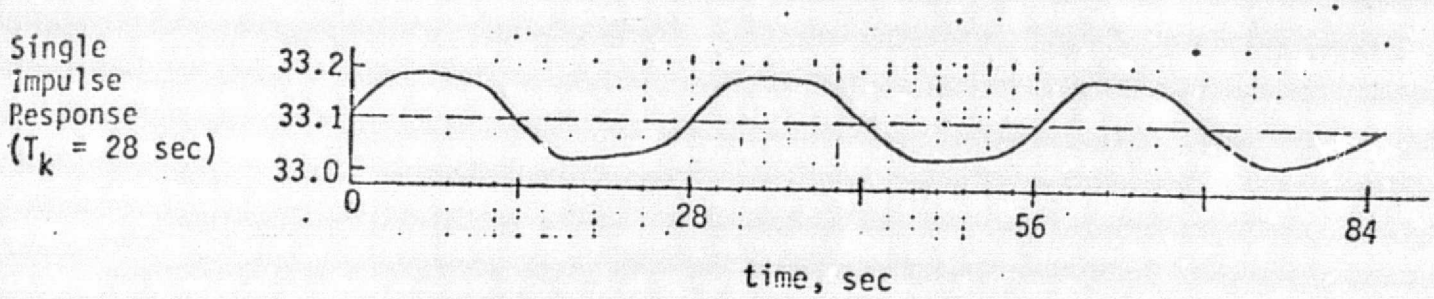

(a) Relative end effector x-position, ft

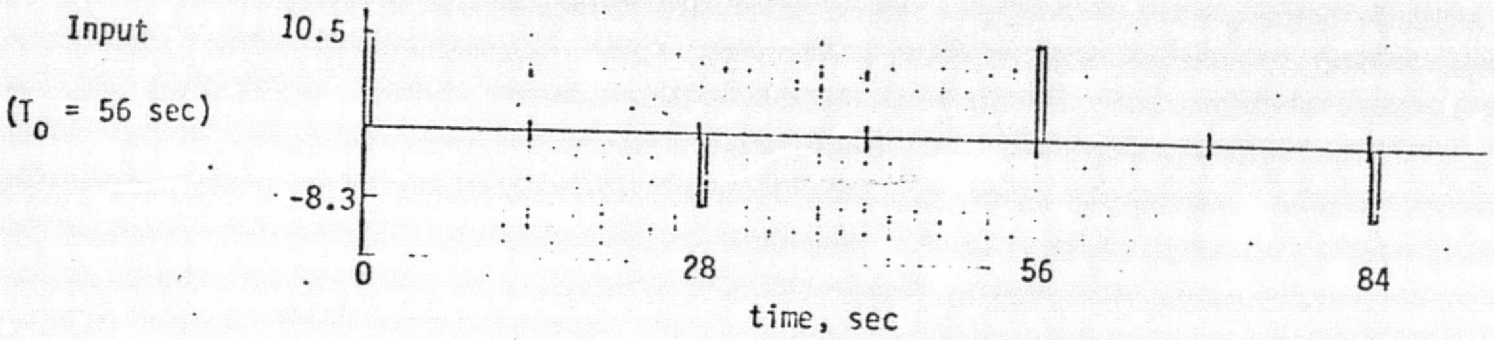

(b) Moment about orbiter y-axis due to PRCS jets, 10^4 ft-lbs

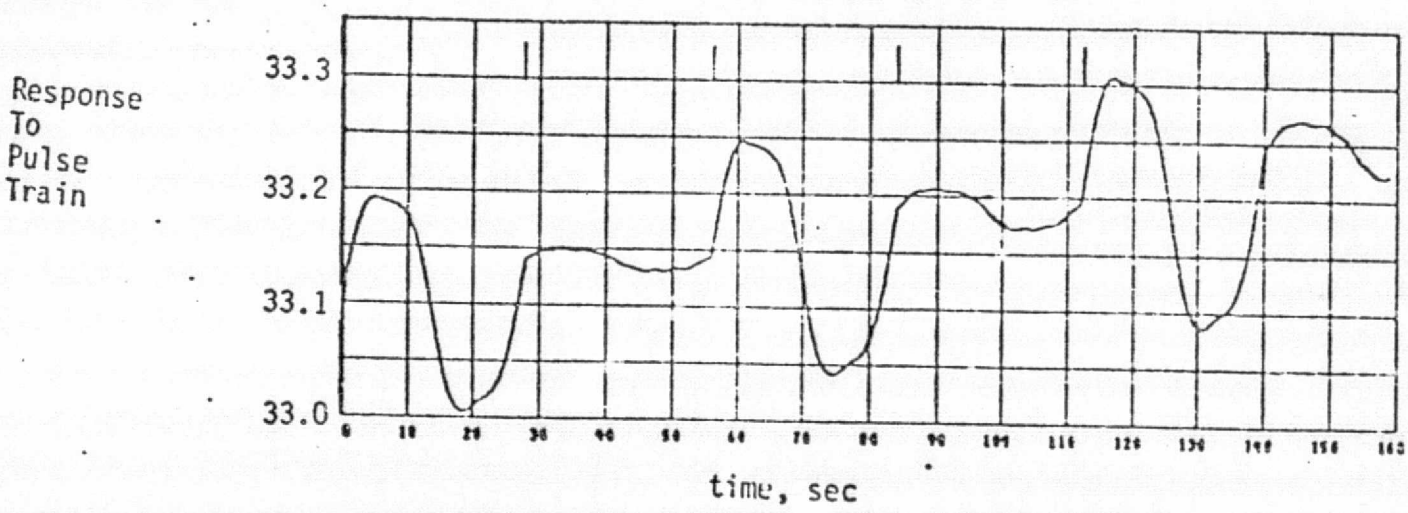

(c) Relative end effector x-position, ft

Figure 21: End effector response to pulse train input
Alternate pulses ($T_o = 2T_k$)

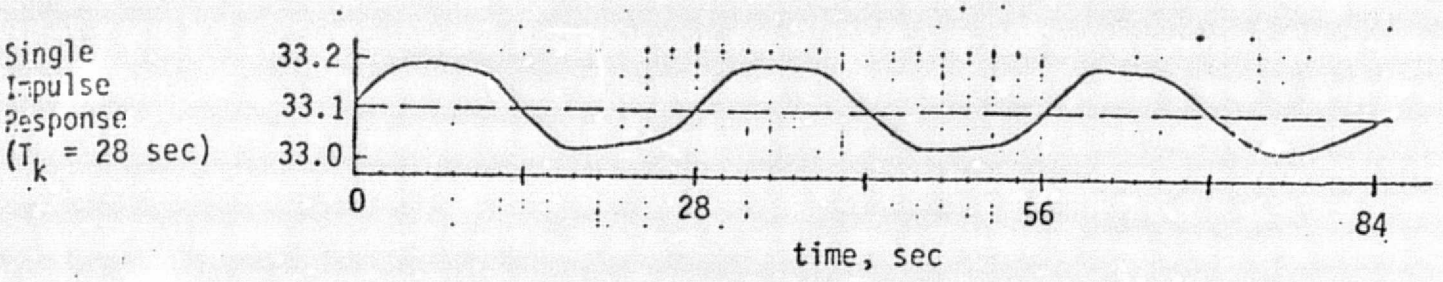

(a) Relative end effector x-position, ft

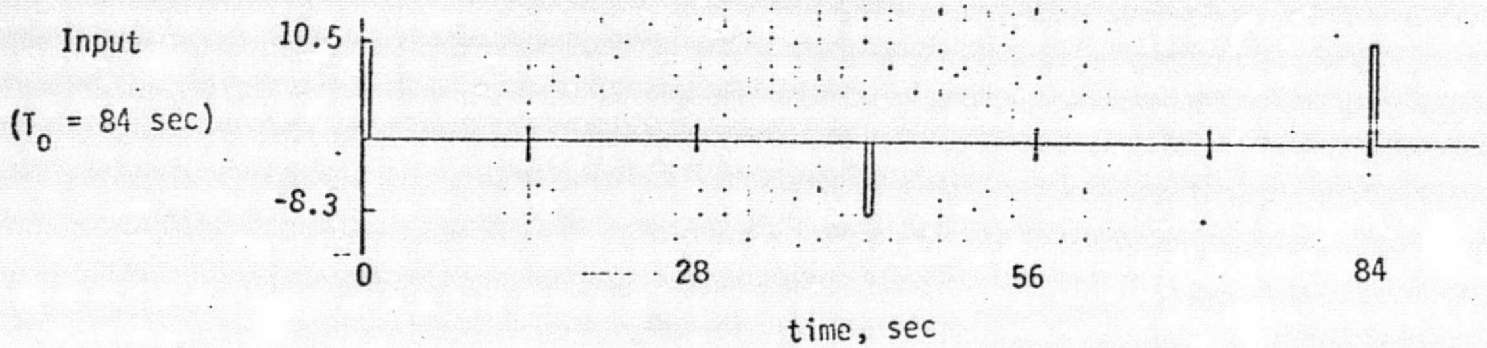

(b) Moment about orbiter y-axis due to PRCS jets, 10^4 ft-lbs

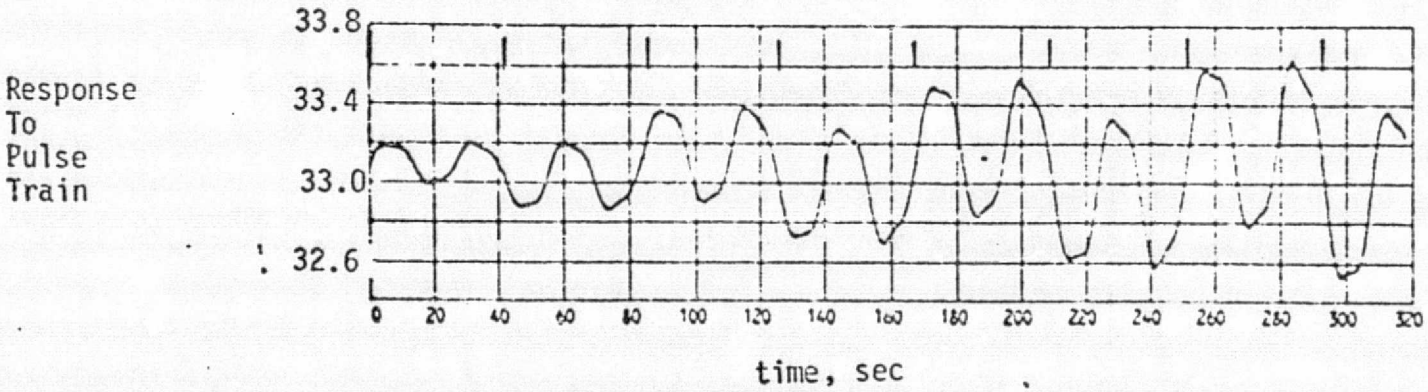

(c) Relative end effector x-position, ft

Figure 22: End effector response to pulse train input
Alternate pulses ($T_o = 3T_k$)

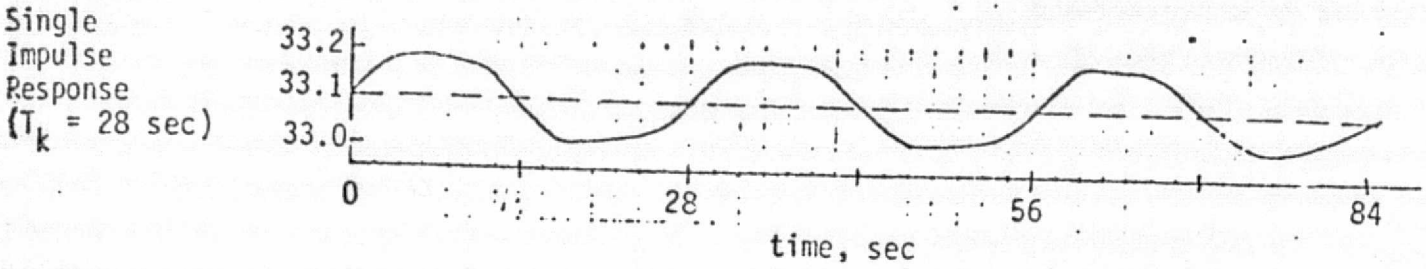

(a) Relative end effector x-position, ft

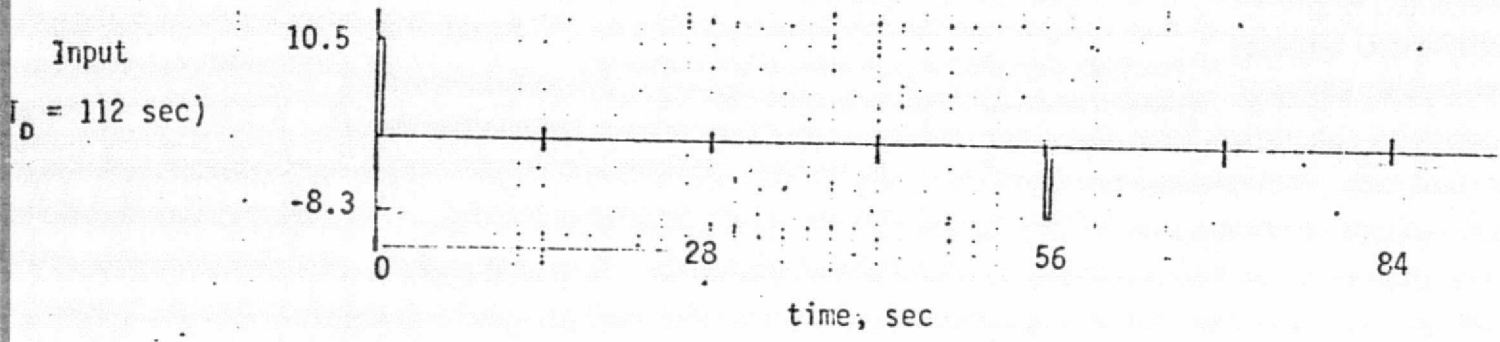

(b) Moment about orbiter y-axis due to PRCS jets, 10^4 ft-lbs

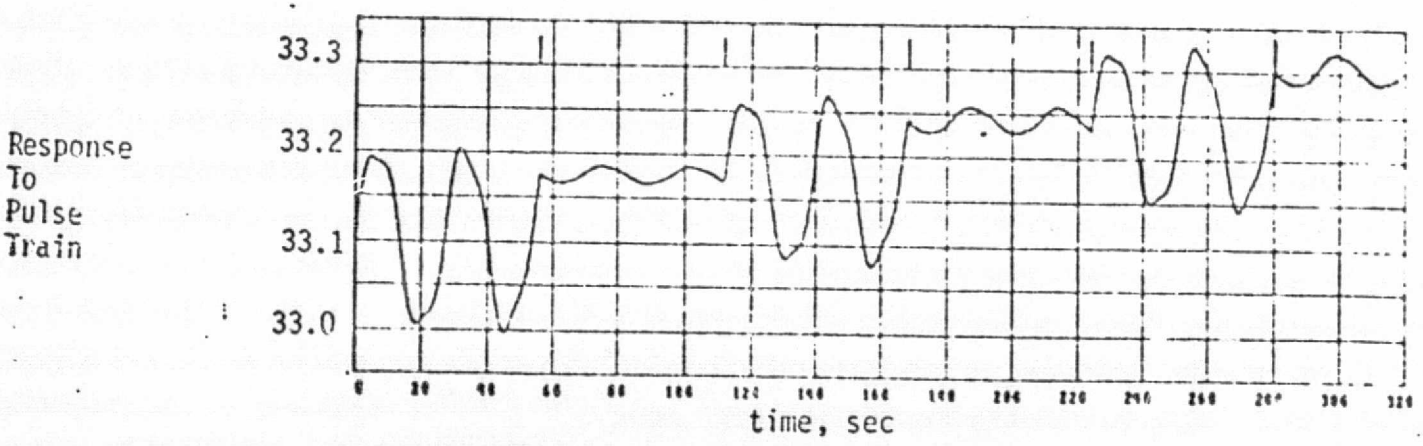

(c) Relative end effector x-position, ft

Figure 23: End effector response to pulse train input
Alternate pulses ($T_O = 4T_k$)

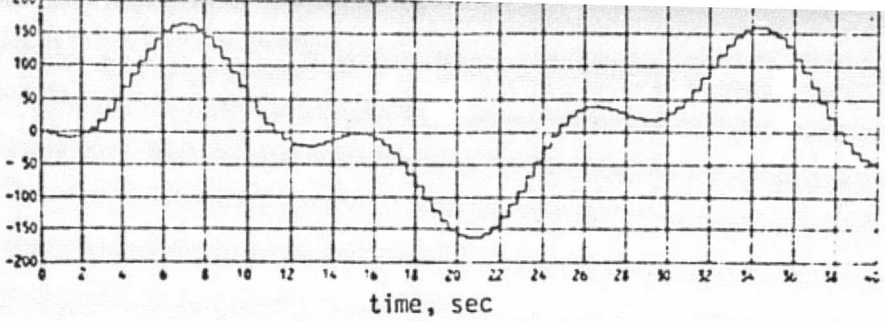

(a) Input: Single pulse

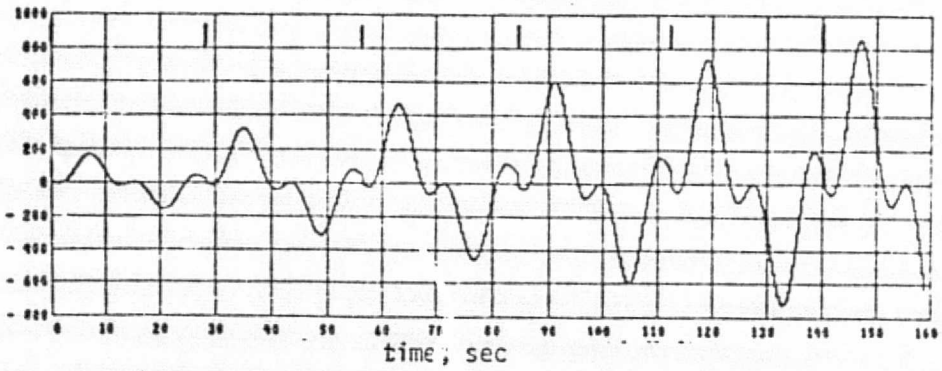

(b) Input: All pulses in positive direction ($T_o = T_k$)

Torque about z, ft-lbs
(hand coordinate system)

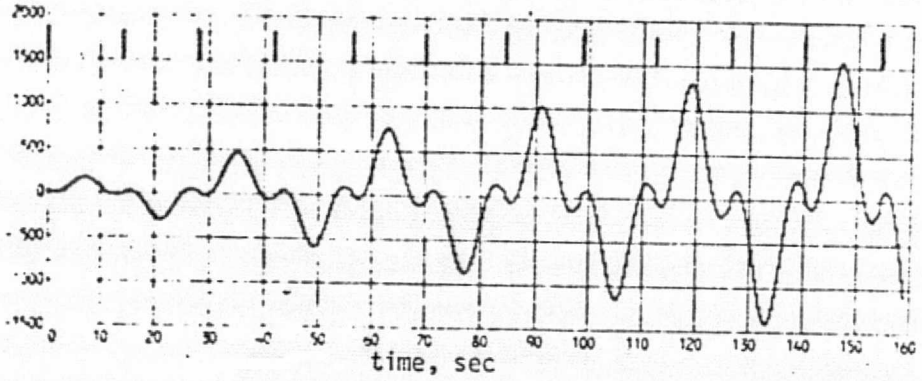

(c) Input: Alternate pulses ($T_o = T_k$)

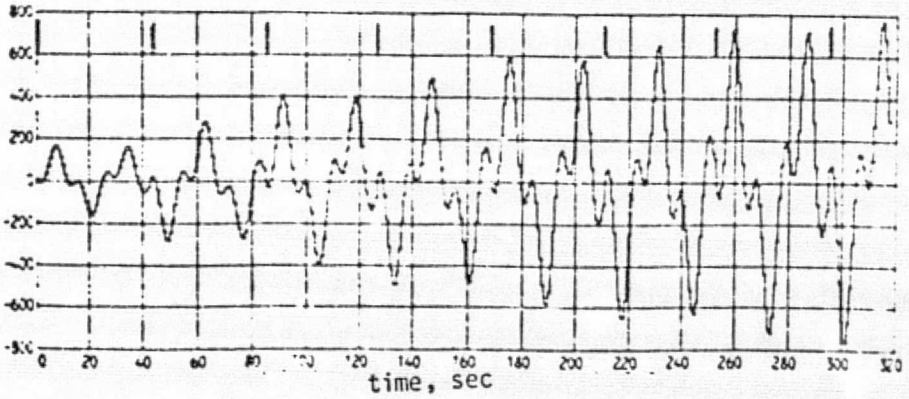

(d) Input: Alternate pulses ($T_o = 3T_k$)

Figure 24: Wrist yaw joint drive axis loads due to pulse inputs about the orbiter y-axis

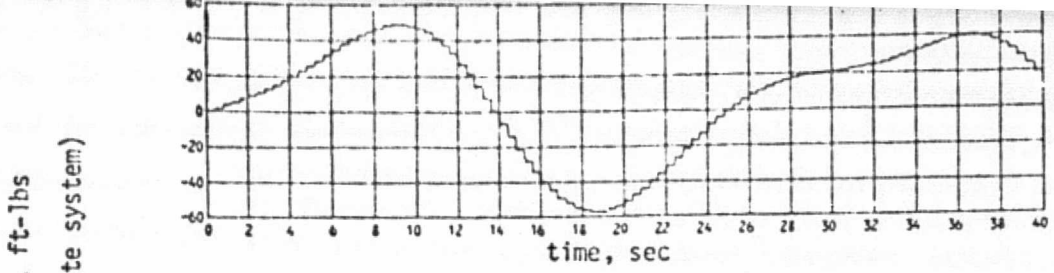

(a) Input: Single pulse

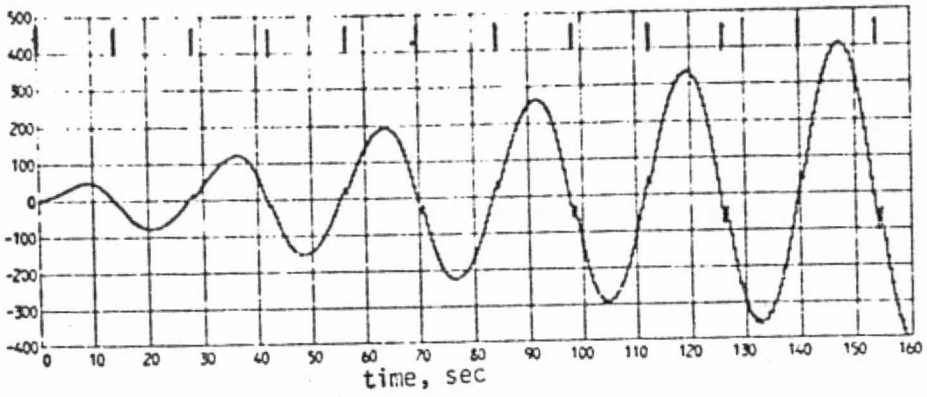

(b) Input: Alternate pulses ($T_o = T_k$)

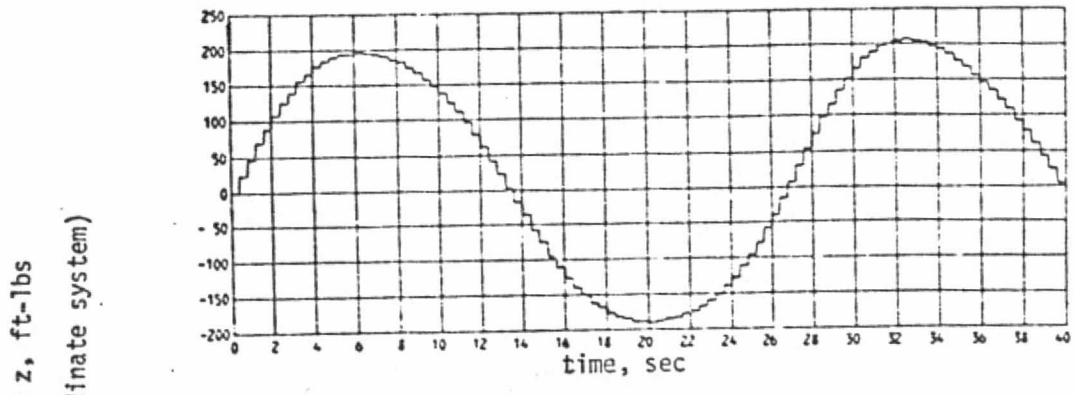

(c) Input: Single pulse

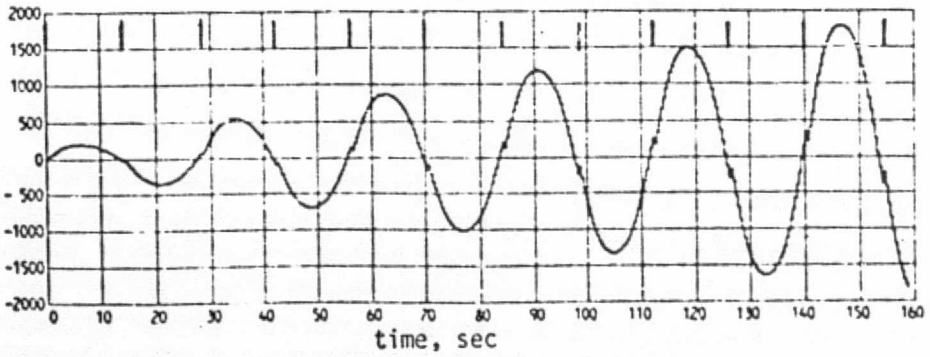

(d) Input: Alternate pulses ($T_o = T_k$)

Figure 25: Elbow pitch joint across axis loads due to pulse inputs about the orbiter y-axis

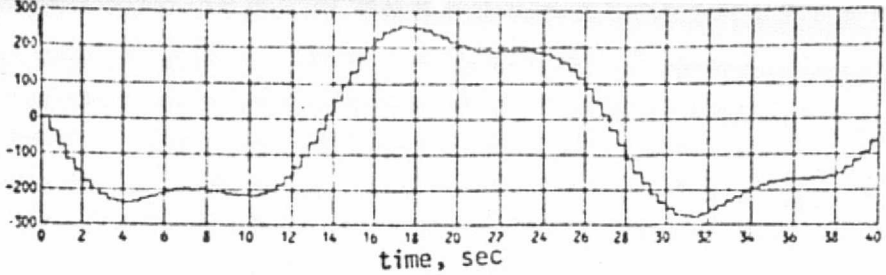

(a) Input: Single pulse

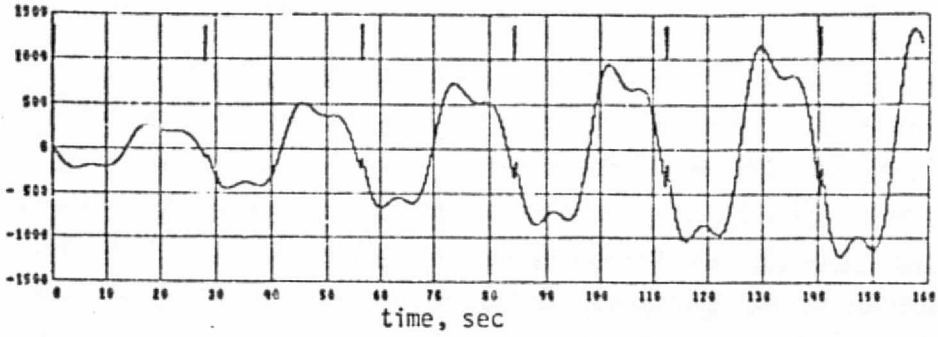

(b) Input: All pulses in positive direction ($T_o = T_k$)

Torque about x, ft-lbs
(shoulder yaw coordinate system)

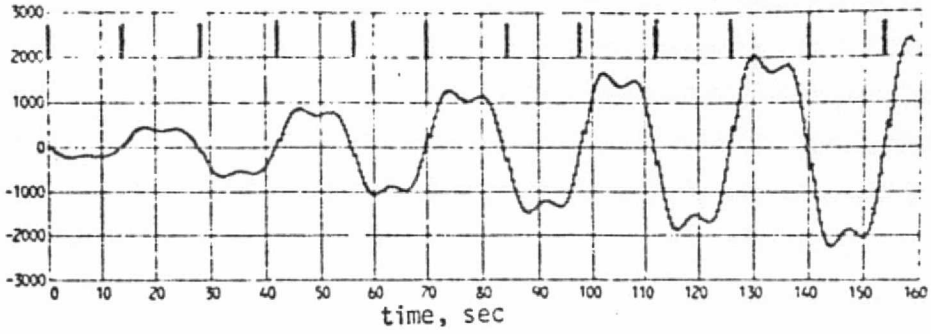

(c) Input: Alternate pulses ($T_o = T_k$)

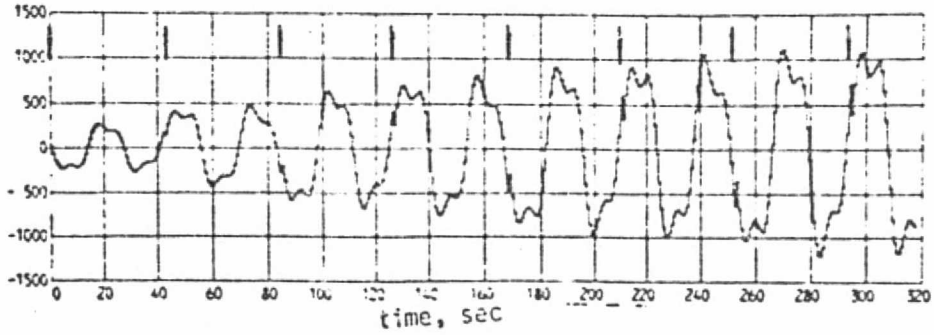

(d) Input: Alternate pulses ($T_o = 3T_k$)

Figure 26: Shoulder yaw joint cross axis loads due to pulse inputs about orbiter y-axis

TABLE 7: SUMMARY OF LOAD RESPONSES TO PULSE TRAIN INPUTS

JOINT	MOMENT	MEAN OPERATIONAL LOAD (FT-LBS)	NO OF PULSES INPUT BEFORE DESIGN LOAD EXCEEDED (ALT PULSES $T_o = T_k$)
WRIST YAW	M_Z*	300	2
ELBOW PITCH	M_X	300	9
	M_Z	1350	9
SHOULDER YAW	M_X	1250	6

* DRIVE AXIS

6.0 Conclusions and Recommendations

This study showed that PRCS step inputs with a loaded arm quickly exceeded the SPAR maximum operational loads. For the roll maneuver the shoulder joint cross-axis reached its maximum operational load in approximately one second.

The results also showed that a single isolated 40 msec minimum impulse PRCS jet firing was acceptable. The resulting loads did not exceed the SPAR mean operational loads.

This study also demonstrated that the passive arm model could be driven unstable with pulse train inputs. Even though the sequence of pulses commanded by the pilot will be random, the sequence is expected to contain some periodic components. Therefore, the response of the arm to periodic pulse trains is of significance.

For the cases with divergent arm oscillations the joint torques quickly exceeded the SPAR mean operational loads. The wrist joint reached its design load after only two pulses.

The results from the study are based on assumptions of massless links, locked joints and elastic torques applied at the joints. Based on the above assumptions it appears that a short pulse train could damage the arm. However the effects of the torque motors were not considered. Therefore, in view of the potential problem identified, it is recommended that this analysis be extended to evaluate the effects of the active joint servo motors.

7.0 References

1. Lockheed Electronics Co: User's Guide for Payload Deployment and Retrieval Systems Simulation (PDRSS) Program, JSC-12658, LEC-10989, August 1977.

2. Lockheed Electronics Co: RMS Massless Arm Dynamics Capability in the SVDS, JSC-12632, LEC-10633, June 1977.

3. Mission Planning and Analysis Division: Shuttle Program Space Vehicle Dynamics Simulation (SVDS) Program User's Guide, Vol II, Rev 2, JSC Internal Note No. 76-FM-26, October 1977.

4. Rockwell International: Guidance Navigation and Controls Verification/ Certification Plan, Vol II Integrated GN&C Book 2 Ascent, SD74-SH-0043-2-2, September 1977.

5. Operational Data Branch: Shuttle Operational Data Book, Vol I, Shuttle Systems Performance and Constraints Data. JSC-08934, Amendment 63, September 16, 1977.

6. Theobald, R. T.: Simplified Analytical Model of Orbiter/RMS/Payload System, Unpublished.

7. SPAR Document No. SPAR-SG.409, Issue C, Load Specification SRMS Manipulator Arm, November, 1977.

8. JSC Memo, MP/77-M297, JSC Evaluation of the SPAR Study on RCS/RMS Interactions, August 24, 1977.